UNIVERSITY OF CRETE

DEPARTMENT OF MATERIALS SCIENCE AND TECHNOLOGY

Rheology of polystyrene melts with various molecular weight distributions

Supervisors
Prof. D.Vlassopoulos
Dr D.Parisi

Bachelor thesis by
Georgios Fragkiadakis

Heraklion, Grecce
February, 2022

Acknowledgments

First of all, I would like to thank from the deepest of my heart my supervisor Professor Dimitris Vlassopoulos. His is one of the most inspiring and motivating persons in my life. Professor Dimitris Vlassopoulos introduced me to the world of Polymer Physics at the University of Crete and gave me the opportunity to work in the Polymer and Colloid lab. His contribution to my progress is not limited to this. He trusted me and he gave me the opportunity to work with him, something that I do really appreciate. I am very thankful to have a supervisor who cared so much about my work, and who responded to my questions and queries so promptly. His continuous support and all the helpful guidance have been very much appreciated.

I am also very grateful to Daniele Parisi for working with me all this time. From the beginning of my thesis until the end, even though he was not with us in the lab, he was helping me to understand the field of rheology very patiently and was always there for me whenever i needed assistance and help. His guidance and advice have been invaluable throughout all stages of the work.

I am particular thankful to the rest of my lab mates, for the best welcome possible in the life of the group and the continuous encouragement and care. These past months I felt that they were more than just colleagues and lab mates. I want to especially thank Katerina for all the help in the initial face of my work and all the patience she had with me throughout this whole time and her ability to help me understand this amazing world of polymers, Consiglia who was always there for me when I had a question and helped me a lot through our discussions to understand the field of Rheology even better and finally Christina who continently encouraged me to try my best and don't get disappointed when the results was not perfect and for all the talks and assistance she gave me from the begging until the end of this work.

Last but not least, I want to thank my family and friends for their love and support and during all those months and throughout the whole journey of my academic years at the university.

Abstract

In this thesis we examined the linear and nonlinear rheological properties of linear polymers with different molar mass and molar mass distribution. The polymer of choice was polystyrene, a well-known thermoplastic with a wide range of applications. The samples used have molar masses ranging from 3 to 70 kg/mol, and reasonably narrow molar mass distribution (MMD), below 2. By mixing different polymers we obtained blends of different average MMD (up to 5.3). We focused on the role of MMD for the same or different average molar mass, which affects the viscoelastic response significantly. We described the linear viscoelasticity with the tube model, accounting for the dynamic solvent contribution of the small components in the blends via double reptation, and presented scaling analysis for the nonlinear shear properties based on the characteristics of the transient signals as function of the Weissenberg number for the different samples. Our results point to the importance of the shape of MMD on the rheological properties of polymers.

Table of Contents

1.Introduction

Polymers have gain great recognition over the years both at scientific and industrial level. Polymers have gained their respective place under the spotlight for over a century now. Nowadays, the synthesis techniques have reached the highest level and consequently this gives us the opportunity to create well-defined polymers with different and complicated structures and as a result different properties. On the one hand, this is due to the investigation of the interactions of the macromolecule's structures, and on the other, due to the fact that minor changes in architecture lead to materials with different chemical, physical and mechanical properties. During this thesis the polymer of choice was Polystyrene and for this work we have 11 polystyrenes samples, divided in individual/pure and blends. The blends are composed with combining the individual/pure samples in different combinations and fractions shown in Table 1. What is fascinating about our samples is that they have a very complex molecular weight distribution (MWD) as well as an increased polydispersity. The goal of this work is to show the effect of the complex and various molecular weight distribution of the samples and the increased polydispersity in polystyrene. In order to achieve our goal for this work, we studied the linear and the nonlinear viscoelastic response of our samples in a wide range of temperatures on a strain-controlled ARES rheometer and a MCR 702 rheometer (Anton Paar) operating in the strain-controlled mode. Since we aim to perform both linear and nonlinear measurements, we used two different types of geometries. For the linear measurements we used parallel plates (PP) of 8mm and 4mm and for the nonlinear measurements we used cone portioned plate geometry (CPP) of 6mm and 4mm. From the linear measurements we produced the master curves for all of our samples using time temperature superposition principle shown in chapter 4.1 whereas for the nonlinear we performed transient rheological measurements and different shear rates, shown in chapter 4.2, in order to have a clearer idea about the dynamics of our samples. The analysis of the nonlinear data was done by extrapolating different parameters from the transient data.

2.Theoretical Background

2.1 Rheology

The term Rheology was coined by E.C.Bingham and it refers to the study of the deformation and flow of matter[1]. Rheometry is the term used for the measurement of the rheological properties of a material. Rheology is particularly useful in characterizing viscoelastic materials which exhibit characteristics of both elastic and viscous response. Viscoelastic materials also can be divided in two categories: Viscoelastic fluids, which are in a liquid state and when they are subjected to a rapid and large deformation, they are prone to structural change, and the viscoelastic solids, which show a coherence and when a large force is applied, they can be deformed substantially. Polymers are viscoelastic materials.

From a rheological point of view, the most probed flow fields are shear and elongational flows. In extensional flow fluid components flow away or towards from one another. Whereas In shear flow, fluid components shear past one another. Shear flows are commonly used to determine the rheological properties of liquid (Newtonian and Non Newtonian Flow).[2] Shear flow can be depicted as layers of fluid sliding over one another with each layer moving faster than the one beneath it. The uppermost layer has maximum velocity while the bottom layer is stationary[3].The two plates model is used to define the fundamental rheological parameters[4] in shear flow. Rotational rheometers and viscometers are the most common equipment to promote shear flows to a viscoelastic material.

Shear Stress:

Figure 2.1 exhibits a one-dimensional scenario where a fluid is in between two parallel plates, characterized by surface A. The bottom plate is stationary, whereas the top plate is displaced with a force F. We define the shear stress as:

$$\sigma=\frac{F}{A} \quad (2.1)$$

where F is the shear force in N and A the shear area is in m^2. The unit of shear stress in Pa.

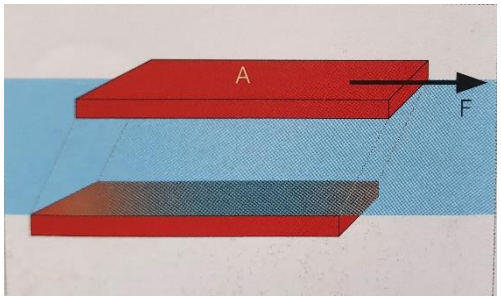

Figure 2.1 Two plates model used to define the shear stress [2].

Shear rate

In figure 2.2 we have again a one-dimensional scenario where a fluid is in between two parallel plates, characterized by surface A and the distance between the two plates is h. The bottom plate is stationary, whereas the top plate is displaced with a velocity v. We define the shear rate as:

$$\dot{\gamma} = \frac{v}{h} \quad (2.2)$$

where v is the velocity in m/s and h is the distance between the plates (see figure 2.2) in m. Shear rate or gamma dot has units of s^{-1}.

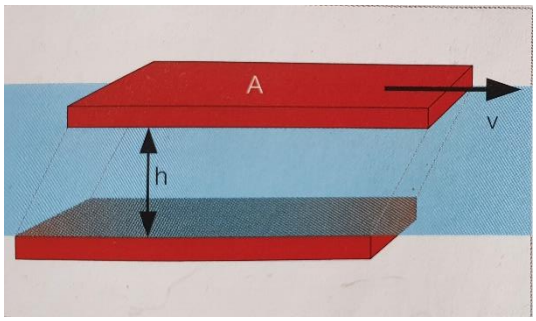

Figure 2.2. Two plates model used to define the shear rate [2].

shear strain

Figure 2.3 exhibits a one-dimensional scenario where a fluid is in between two parallel plates, characterized by a deflection path s and the distance between the two plates is h. The bottom plate is stationary, whereas the top plate is being deflected by a distance s. We define the shear rate as:

$$\gamma=\frac{s}{h} \tag{2.3}$$

where s is the deflection path in m and h is the shear gap in m. Hence the shear strain is dimensionless.

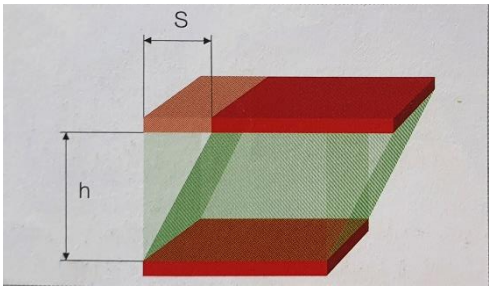

Figure 2.3. Two plate model used to define the shear strain [2].

Under conditions of linear response, the complex G is the ratio of shear stress and strain,

$$G=\frac{\sigma}{\gamma} \tag{2.4}$$

and describes the elastic character of the material. To obtain information about both the elastic and viscous response at once, small amplitude oscillatory shear deformation is applied to a test viscoelastic material. In that case, the modulus of eq (2.4) becomes the complex modulus G* and consists of two contributions, the in-phase storage modulus (G') and the out-of-phase loss modulus (G''). In the case of storage modulus being larger than the loss modulus the sample can be categorized as viscoelastic solid. On the other hand, when loss modulus exceeds the storage modulus the material will be categorized as viscoelastic liquid. The loss factor is the ratio between the loss modulus and storage modulus and is used to describe the ratio of the two portions of the viscoelastic behavior and is dimensional.

$$\tan(\delta)=\frac{G''}{G'} \quad (2.5)$$

Given that polymers are characterized by multiple time and length scales, we use the storage modulus and loss moduli as functions of the imposed frequency of the oscillatory deformation to create a master curve. The frequency represents the inverse experimental time scale within which the material response is probed, and relates to the length scale associated with that response. Hence, the master curve represents that equivalent of a spectroscopic information and this type of linear rheological measurement is often referred to as mechanical spectroscopy. Figure 2.4 shows a typical master curve which is decided in different sections as described now.

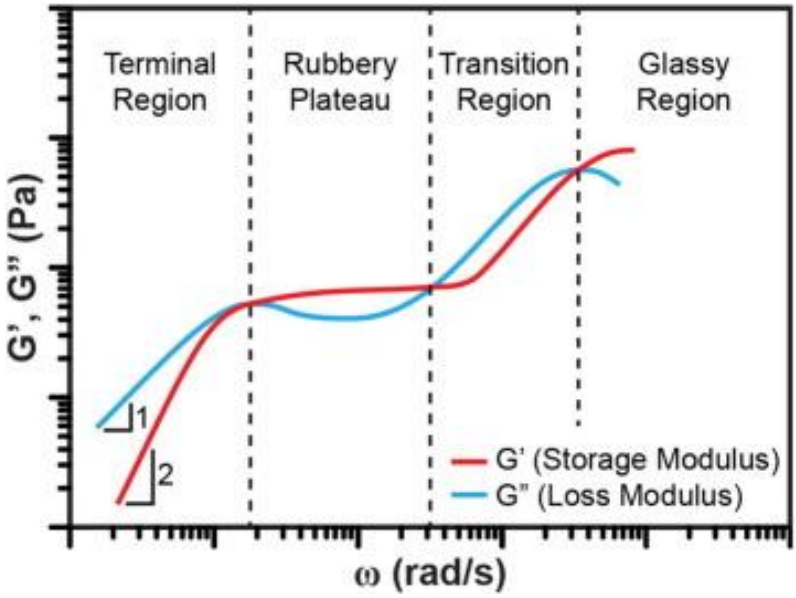

Figure 2.4. A complete master curve [3].

At the lowest frequencies, in the so-called terminal region, the loss modulus (G'') dominates over the storage modulus (G'), indicating a viscoelastic liquid-like behavior. With respect to their frequency dependence, the storage modulus (G') exhibits a power-law slope of 2, and the loss modulus (G'') of 1. On increasing frequency beyond the

terminal crossover of the moduli, a plateau region is observed which reflects the rubbery behavior of the material with G'>G''. It is followed by an intermediate transition regime with local (high frequency, small length) liquid-like response and ultimately the glassy region, where solid-like behavior dominates[5]. At the terminal region polymers can flow and the chains relax. The plateau range varies and depends on the molecular weight.

2.2 Rouse model[6]

The description of polymer dynamics is based on coarse graining, and the bead-spring models where the friction is equidistributed along the chain represent the current state of the art in molecular modeling. For unentangled chains, the Rouse model represents a chain by a sequence of N (degree of polymerization) beads which are connected by springs size b (monomer). The model assumes ideal chains (conforming to the model of Kuhn) and ideal conditions no enthalpic or topological interactions.

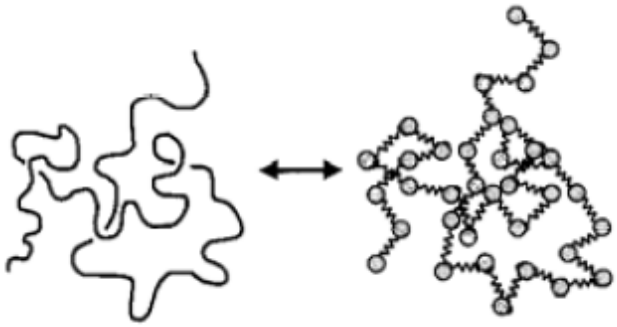

Figure 2.5. A chain of N monomers is mapped into a bead-sprig chain of N beads connected by N-1 springs.[4]

The chains experience a frictional force proportional to their velocity and the total friction coefficient of the Rouse chain is the sum of the contributions of each of the N beads given by:

$\zeta_R = N*\zeta$ (2.6)

The diffusion coefficient of the Rouse chain is given by the Einstein relation:

$D_R = \frac{K_B T}{\zeta_R}$ (2.7).

The Rouse time (τ_R), is the ratio between the mean square displacement of the chain (with end-to-end distance R) and the diffusion coefficient of the chain. So, Rouse time is given by the following equation:

$$\tau_R=\frac{R^2}{D_R}=\frac{\zeta N R^2}{KT}=\tau_o N^2 \quad (2.8).$$

Where τ_o is the relaxation time of the Kuhn monomer

$$\tau_0 \approx \frac{\zeta b^2}{K_B T} \approx \frac{n_s b^3}{K_B T} \quad (2.9)$$

For times smaller than τ_R, polymers have a viscoelastic behavior and for times longer than τ_R, the polymers exhibit the response of a liquid.

2.3 Zimm model[6]

The Rouse model works for unentangled polymer melts but not for dilute polymer solutions (isolated coil). In the latter case, the model of Zimm takes into consideration the hydrodynamic interaction which is the long-range force acting on a particle, mediated solvent that arises from motion of one particle.

The friction coefficient of the chain depends on the viscosity of the solvent η_s and is given by Stokes law:

$$\zeta_Z=\eta_s R \quad (2.10)$$

The diffusion coefficient of a chain in the Zimm model is:

$$D_z \approx \frac{K_B T}{\eta_s R} \quad (2.11)$$

The Zimm relaxation time given by the model:

$$\tau_z \approx \frac{R^2}{D_z} \approx \frac{\eta_s R^3}{K_B T} \approx \tau_o N^{3/2} \quad (2.12)$$

2.4 Tube model

The diffusion of a long test chain in a dense polymeric system is highly constrained. The chain is entangled with the neighboring chains, and its lateral motions are topologically prohibited as shown in figure 2.6 below.[7]

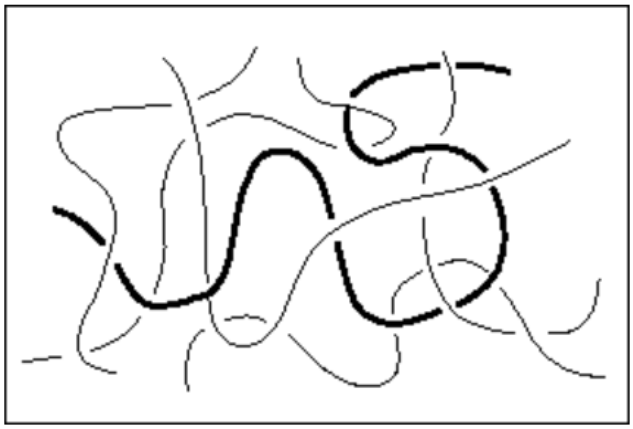

Figure 2.6.A test chain (thick line) confined by neighboring chains (thin line)[5]

The constraints exerted by the neighboring chains onto the test chain, can be described by the tube model and the inhibition of later motion is the so-called uncrossability condition. The tube concept due to Edwards, opened the route for the successful description of the complication motion of long chains in a sea of entanglements. This is the so-called reputation model of De Gennes.. [8,9]

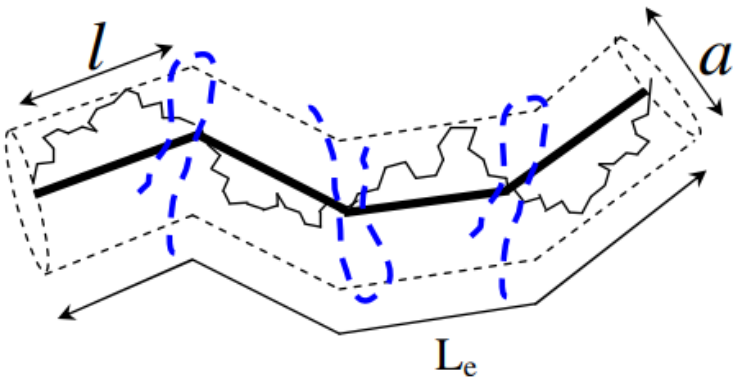

Figure 2.7 : Schematic representation of a chain in the tube. Real chain: thin broken line; primitive path: thick line; entanglements: dotted line [7].

The chain is constrained within the tube, whose curvilinear axis is the primitive path of the chain. The primitive path comprises a sequency of blobs, each have degree of polymerization $N_e=\frac{M_e}{M_o}$ (of an entanglement segment). The tube diameter α (locus of constraints by neighbors) is the blob diameter, shown in figure 2.8 and is given by

$$\alpha \approx b\frac{M_e}{M_o} \tag{2.13}$$

where M_e is the entanglement spacing and M_o is the molecular weight of a Kuhn monomer of size b.[10]

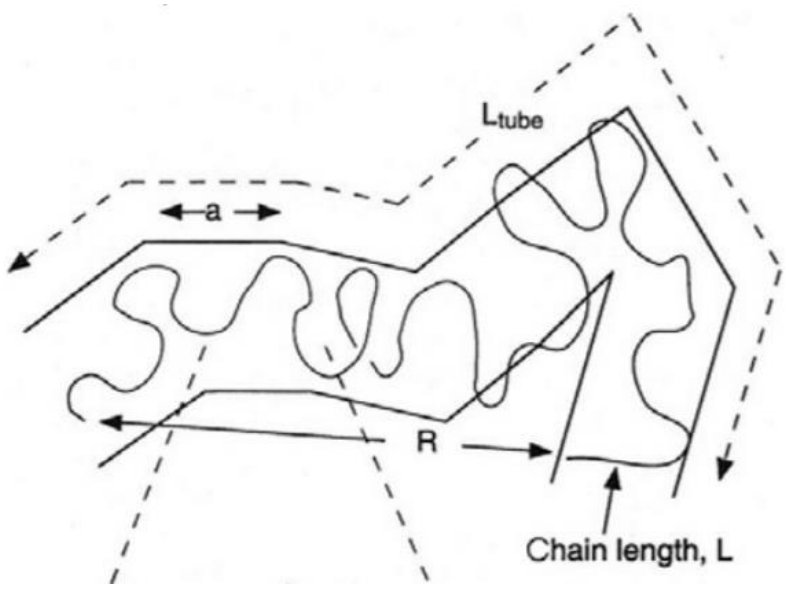

Figure 2.8.A sketch of tube showing definitions of length scales in the tube model [7]

The primitive path of the tube consists of N/N_e parts of size α, so eventually, we can write the following equation about its end-to-end distance:

$$L \approx \alpha \left(\frac{N}{N_e}\right) \tag{2.14}$$

The relaxation of a chain in a tube is performed via curvilinear diffusion of the primitive path and the process is known as reptation. Every time a portion of the tube is vacated by the chain, that portion of the tube is "forgotten" as shown in figure 2.9

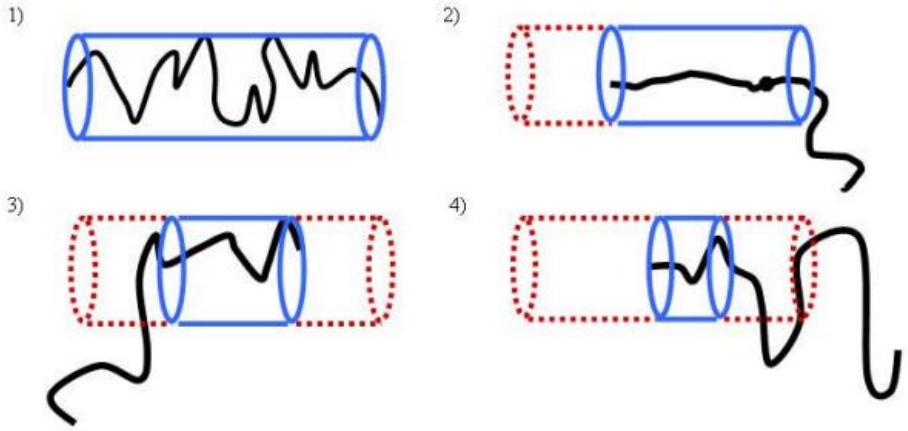

Figure 2.9. Reptation model, the parts that are left empty disappear[6].

The curvilinear diffusion coefficient, D_c, is given by:

$$D_c=\frac{K_BT}{N\zeta} \tag{2.15}$$

The time it takes for the chain to diffuse out of the tube is called *reptation time*:

$$\tau_{rep}\approx\frac{R^2}{D_c}\approx\frac{\zeta b^2N^3}{k_BTN_e}=\frac{\zeta b^2}{k_BT}\cdot {N_e}^2\cdot(\frac{N}{N_e})^3 \tag{2.16}$$

Note that, experiments showed that beyond a critical value of molar mass $M_C\approx M_e$ the relaxation time scales as $\tau \sim M^{3,4}$ where the difference between 3 and 3.4 is significant for large M. The reason for this mismatch is that the action of additional relaxation mechanisms, in particular contour length fluctuations (pioneered by Doi based on early ideas of De Gennes) and constraint release (pioneered by Rubinstein, Colby, De Cloizeau and Tsenoglou [6]. Figure 2.10 shows zero shear viscosity data collected by Berry and Fox on a wide range of polymeric systems, where it can be noted that above a critical value of molar mass the slope from 1 (Rouse) increases to 3.4 for a wide range of polymers. This trend was found independent on the polymer chemistry.

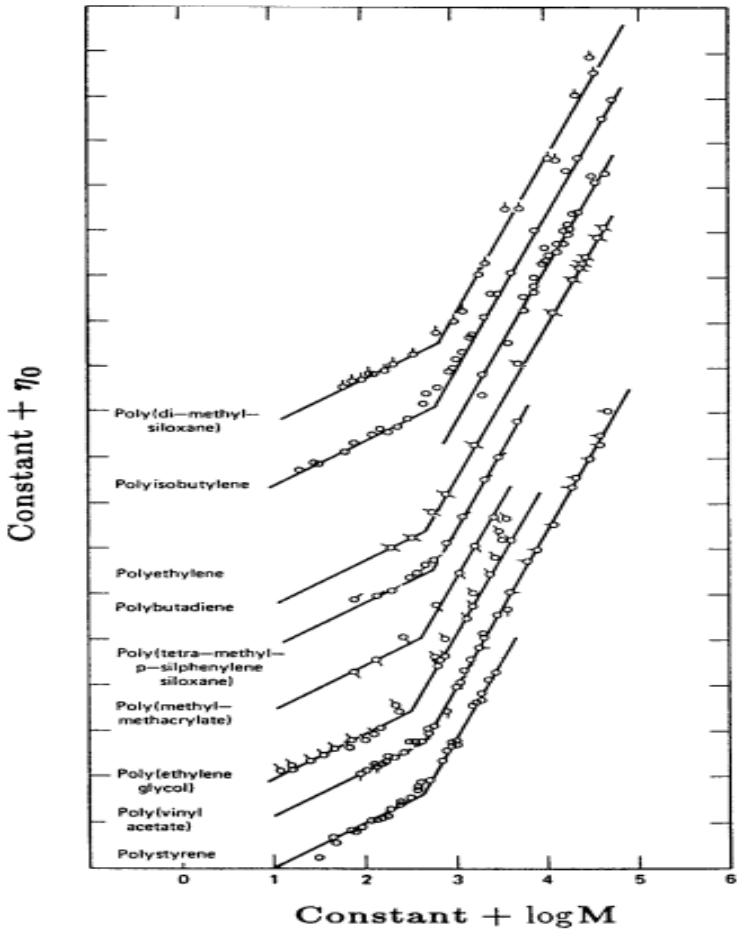

Figure 2.10. Relationship between zero-shear viscosity and molecular weight for several nearly monodisperse melt samples where we can see that from a critical molar mass, M_c, the slope from 3 goes to 3,4. [7]

Concerning the mechanism of "contour-length fluctuations" (CLF), seen in figure 2.11, the action is at the chain end-segments which have more degrees of freedom and relax faster compared to the central segments which reptate. Hence the overall chain relaxes faster with partial reputation and CLF compared to full reputation. In addition, since the portion of end-segments changes with M, the M-dependence of this combined relaxation is stronger compared to full reputation.

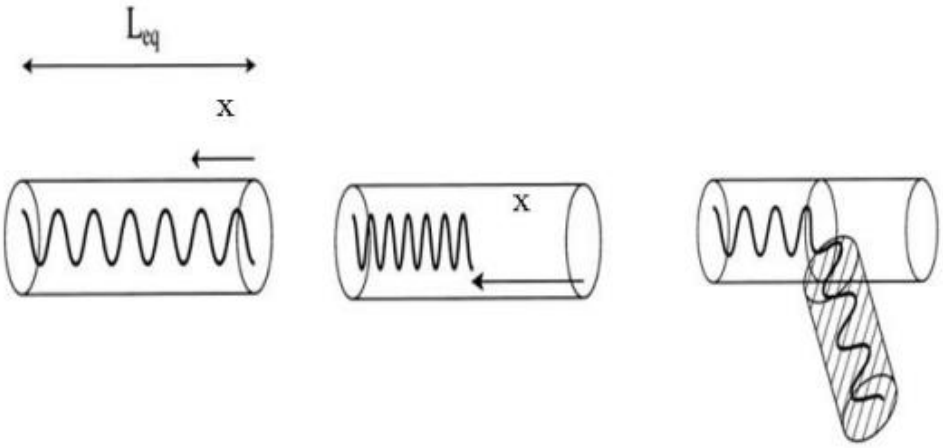

Figure 2.11 : Contour Length Fluctuations process [7]

3. Materials and methods

The samples used in this work are polystyrenes, synthesized by radical polymerization and have been provided by Professor Michael Monteiro from the University of Queensland, Australia. The samples are polydisperse linear polymers and their blends. Details about the samples, the polydispersity index (PI) and glass transition temperature of the samples are provided in Table 1.

Table 1: List of samples and their characteristics in this thesis.

SAMPLES	Blend composition (mg)	Mn (g/mol)	PI	Tg (^{o}C)
SB1	A (28.1) D (71.7)	6200	2.41	88
SB2	B (37.3) E (62.7)	22460	2.50	97.5
SB3	C (16.7) D (45.8) E (37.5)	16590	2.64	96
SB4	C (23.4) D (13.1) F (64.0)	30670	2.92	99
SB5	A (49.8) B (21.1) E (28.9)	5710	5.30	89
S6	A	3240	1.84	77
S7	B	11870	1.85	95
S8	C	21230	1.81	99
S9	D	9090	1,95	95
S10	E	41450	1.85	103
S11	F	70400	1.82	104

The Gel permeation chromatography (GPC) method is used widely to measure molecular weights of linear polymers. High-quality GPC data contains detailed information on many aspects of the polymer's molecular weight distribution (MWD)[11]. Gel permeation chromatography (GPC) is a type of size-exclusion chromatography (SEC), that separates analytes on the basis of size. The separation is based on the elusion time of the different sizes. Figure 3.1 shows the MWD of SB5 and its pure components as well as the fraction of each component for the preparation of the blend. The rest of the GPC figures are presented in the Appendix.

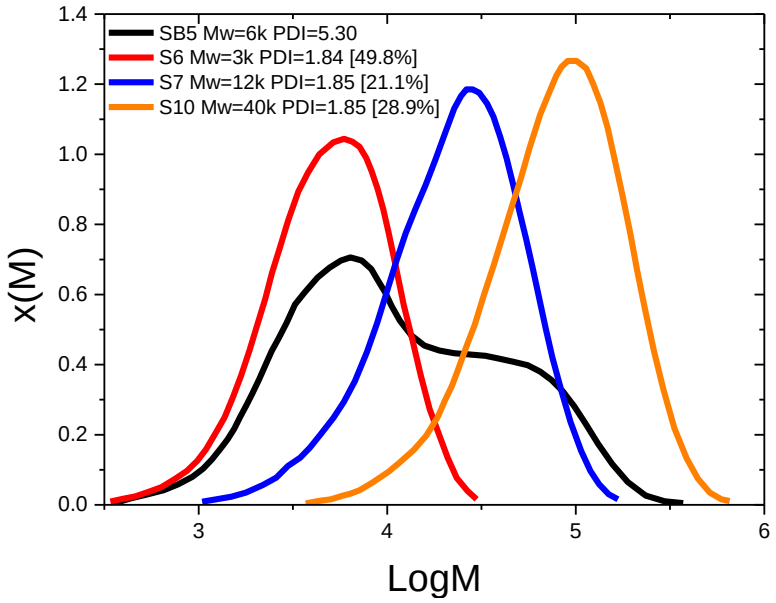

Figure 3.1. MWD of samples SB5, S6, S7 and S10 and their fractions in the blend.

The glass temperatures values (T_g) were measured by means of differential scanning calorimetry (DSC). Figure 3.2 exhibits all the Tg traces for all samples, for the second run of the heating scans at 10 ^oC/min.

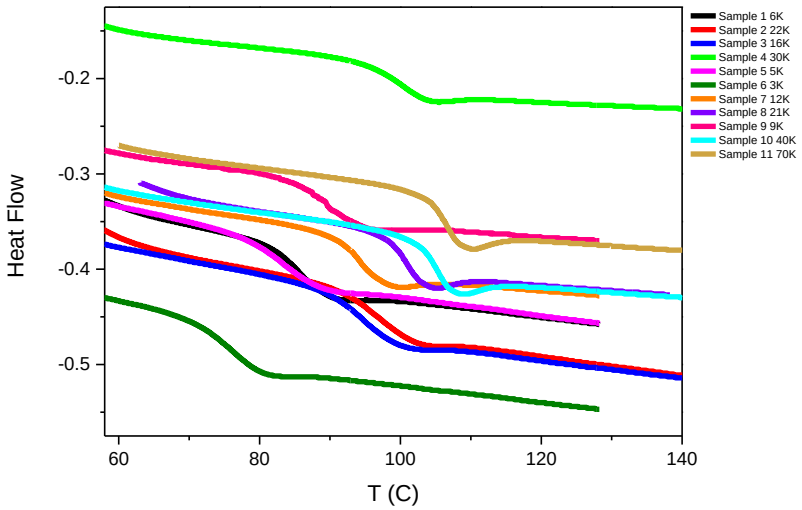

Figure 3.12.DSC heating curves of all the samples studied. The curves are the second heating scans at 10 ^oC/min

The samples were shaped in a disc form with the hydraulic press and placed in the oven for annealing overnight under vacuum at 150 ^{o}C. Afterwards the samples were reshaped to 8mm or 4mm discs using the hydraulic press under vacuum. The samples were heated to Tg+50^{o}C for 30 minutes. Subsequently the samples were pressed using either the hydraulic press or the manual press in order to reach their final shape. This procedure was necessary to ensure that the samples were completely homogenous and without any form of air bubbles inside of the disc. We faced some difficulties in sample preparation especially the low molecular weight samples because they were difficult to handle as they were very brittle and broke quite easily.

3.1 Rheological Measurements

Rheological measurements were performed on a strain-controlled ARES rheometer (TA Instruments) equipped with a force rebalance transducer 2KFRTN1 and a convection oven, ensuring accurate temperature control (0.1±^{o}C). For the experiments, a stainless-steel plate-plate geometry see figure 3.3 with diameters of 8mm and 4mm diameter was used. The 4mm geometry was necessary for low-temperature measurements near the glass transition, where the sample became stiff. The samples were loaded into the rheometer and allowed to melt and homogenize at temperatures ranging from 140^{o}C to 160^{o}C for around 60 min. In addition, a, MCR 702 rheometer (Anton Paar) operating in the strain-controlled mode, was also used. This rheometer is equipped with a CTD-180 hybrid oven, which provides a temperature control (±0.1^{o}C) by means of Peltier and convection system. The same procedure as with the ARES rheometer was followed.

12

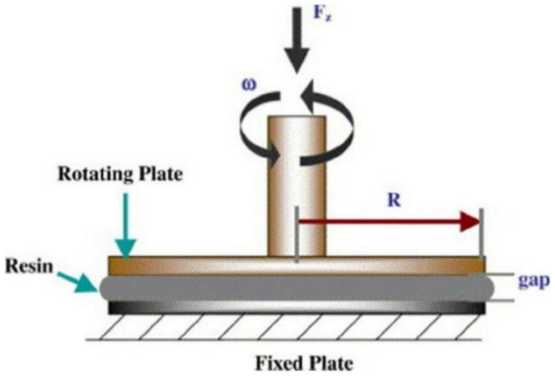

Figure 3.13. Parallel plate geometry
[1]

As already mentioned, for stiff samples we chose a 4 mm diameter plate to reduce the effects of the instrument compliance (further details are provided below). On the other hand, the 8 mm plate was used for the highest temperatures of the measurements mainly for the fact that with the 8mm we had better torque resolution.

For the nonlinear rheological measurements, a cone partitioned plate (CPP) geometry was utilized, figure 3.4 and figure 3.5. Rheological measurements were performed on a strain-controlled ARES rheometer (TA Instruments) which the CPP was mounted. A correct and good alignment of inner and outer partition was ensured before we proceeding with the rest of the experiment. The whole setup was left in the oven for at least 45 minutes for thermal equilibration and subsequently we calibrated the gap at the chosen temperature. Afterwards we proceeded with the loading of the sample and annealing it for at least one hour for sample thermal equilibration. Then we proceed with adjusting the gap to the appropriate value, paying close attention to the normal force, which should not exceed the equivalent of 100g in weight. Finally, we were ready to proceed with the measurements. [13,14]

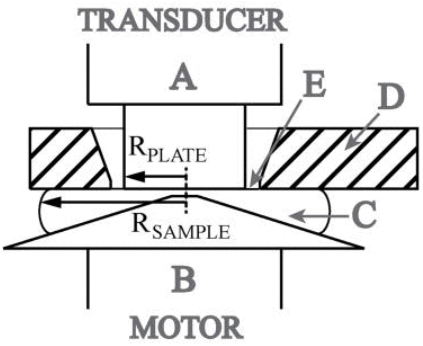

(a)

Figure 3.14.C the loaded sample, D the outer stationary ring (partitioned-plate), E the gap between the outer ring and the upper plate [2]

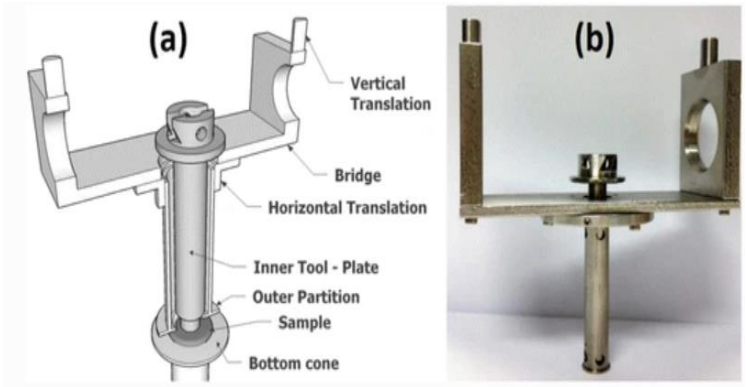

Figure 3.15. Cone partition plate setup [3]

For these measurements the temperature of choice was selected from the linear viscoelastic data. We targeted an appropriate temperature where samples exhibit both a solid-like and a liquid-like behavior (i.e., viscoelastic). We used 4 mm and 6 mm diameter discs. However, obtaining good and reliable data from the non-linear measurements is not something easy. In general, the sheared viscoelastic material may be prone to instabilities such as fracture of the sample's edge (at the material/air interface), wall slip and shear banding. Shear banding is observed when two different shear rate regions form with different velocity profiles under the same externally imposed shear field. [15]

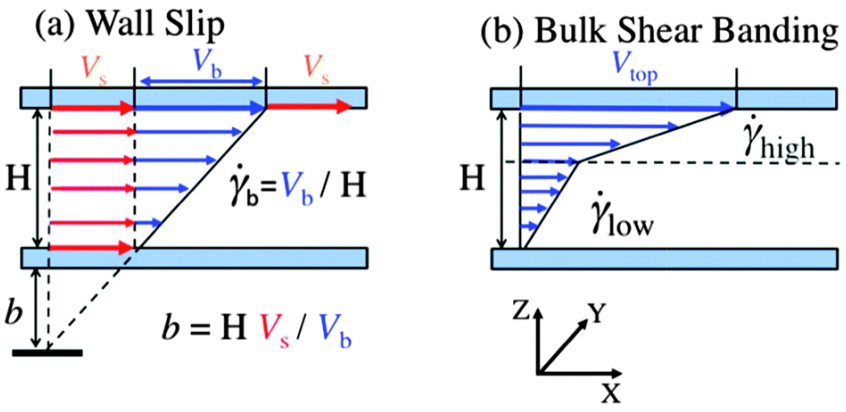

Figure 3.16. (a) wall slip and (b) shear banding [4]

Wall slip is usually caused by large velocity gradients in a thin region adjacent to the wall shown in figure 3.6. When wall slip occurs, the measured viscosity can be significantly lower than the actual viscosity of the sample. To overcome this effect, roughened surface are typically used[16]. Edge facture has been studied over the years and the key finding is that it originates from the second normal stress difference N_2 when it exceeds the respective stress associated to the interfacial tension at this edge.[17] Figure 3.7 is a visual representation. At high rates the edges of the sample start to deform inside the sample. This leads to fracture propagating inside the sample affecting the measurement.

Figure 3.17. (a) A visual show of the edge fracture in cone plate[2]. (B) an image of edge fracture in a sample.

The specific tests performed are described below.

3.1.1 Dynamic Strain Sweep (DSS) Tests

During the strain sweep tests the angular frequency and temperature were held constant throughout the measurement and the strain amplitude varied. At low values of the strain amplitude, the values of the storage and loss moduli G'(ω) and G''(ω) respectively do not depend on the strain. This is the linear viscoelastic (LVE). Beyond a critical value of the strain the moduli of G' and G'' are not constant anymore, see figure 3.8. This marks the non-linear viscoelastic region, where the structure (e.g., chain conformation) of the sample is affected. From the DSS tests we were able to determine the value of strain in which we are in the linear viscoelastic regime, to perform LVE measurements.

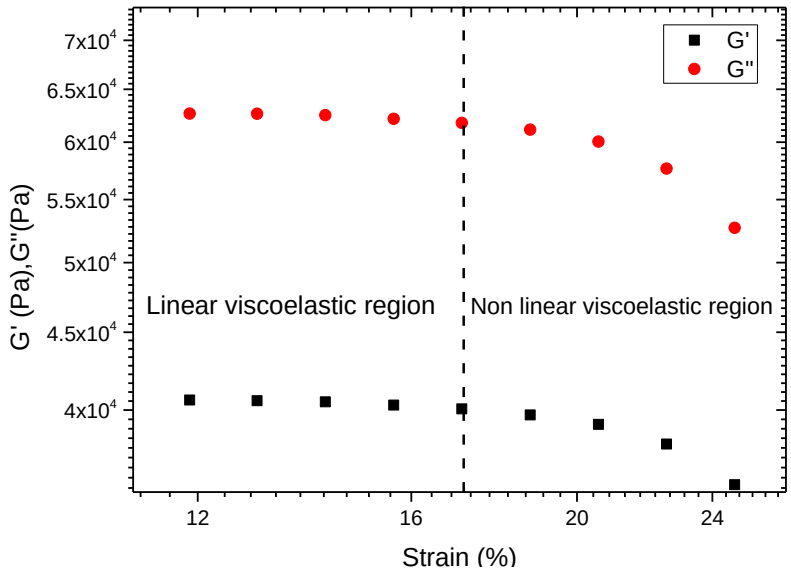

Figure 3.18. Dynamic Strain Sweep Test Sample 7 12.000Kg/mol at T=150 °C and frequency 100rads/sec

3.1.2 Dynamic Frequency Sweep (DFS) Test and Time Temperature Superposition

Here we keep a constant chain amplitude in the LVE regime and vary the angular frequency. In order to explore the time dependent deformation behavior. The DFS test provides the viscoelastic properties of a sample at different frequencies, which reflect relevant material timescales. Several parameters can be obtained, such as the Storage (Elastic) Modulus (G'), the Viscous (Loss) Modulus (G"), loss factor tan(δ) G''/G' where δ is the loss angle and the Complex Viscosity (η*), in the frequency ranged from 10^2 rad/s to 10^{-2} rad/s.

Time Temperature Superposition (TTS) is a well-known procedure to determine the temperature dependance of the rheological behavior of a polymer by expanding its dynamic range at a given temperature at which we study the material.[18] TTS is implemented by shifting the LVE data obtained at several temperatures to a common reference temperature (T_{ref}) until they collapse based on the reference temperature. Data can be shifted with the use of horizontal shift factor (α_T) and vertical shift factor(b_T). Whereas this is an empirical approach ,α_T reflects primarily the temperature dependence of the segmental friction coefficient[19]. The function α_T is thus a very important one in describing the physical properties of a polymer system and determines the time scale and reflects the temperature dependence of diffusion coefficient D (with ζ being the monomeric friction).

$$(\alpha_T) = \frac{D_{(T_0)}}{D_{(T)}} = \frac{\zeta T_o}{\zeta_o T} \tag{3.1}$$

The horizontal shifting was performed manually by shifting the data until they collapsed with each other. We calculated the horizontal shift factor α_T relying to the tan(δ) plot versus frequency by overlapping the data of the selected range of temperatures to the selected reference one.

The vertical shift factor results from the temperature dependence of product of density and absolute temperature[20]. The modulus scale factor, b_T is given from the equation:

$$b_T=\frac{\rho_{ref}T_{ref}}{\rho*T} \quad (3.2)$$

where ρ is the temperature dependent density and for polystyrene is given by this equation:[21]

$$\rho(T)= 1.2503 - 6.05x10^{-4}T[K] \text{ in } g/cm^3 \quad (3.3)$$

The true shear strain applied to the sample is always lower than the command (motor) strain because the test fixtures and the torque transducer are also deformed by the stress, required to shear the sample. If the sample/ geometry configuration is stiff compared to the instrument, instrument compliance effects become significant and need to be corrected.[22]

In order to correct the instrument compliance, we use the following equations:

$$G'_s = \frac{G'_m\left(1-\frac{J_i}{k_g}G'_m\right)-\frac{J_i}{k_g}G''^2_m}{(1-\frac{J_i}{k_g}G'_m)^2+(\frac{J_i}{k_g}G''_m)^2} \quad \text{for the storage modulus G'} \quad (3.4)$$

$$G''_s = \frac{G''_m}{(1-\frac{J_i}{k_g}G'_m)^2+(\frac{J_i}{k_g}G''_m)^2} \quad \text{for the loss modulus G''} \quad (3.5)$$

Where J=$\frac{\Theta}{M}$ is the compliance represented by the ratio between the deflection angle and the torque, and, Kg=$\frac{2h}{\pi R^4}$, h is the measuring gap and R is the radius of the geometry used in the measurement.

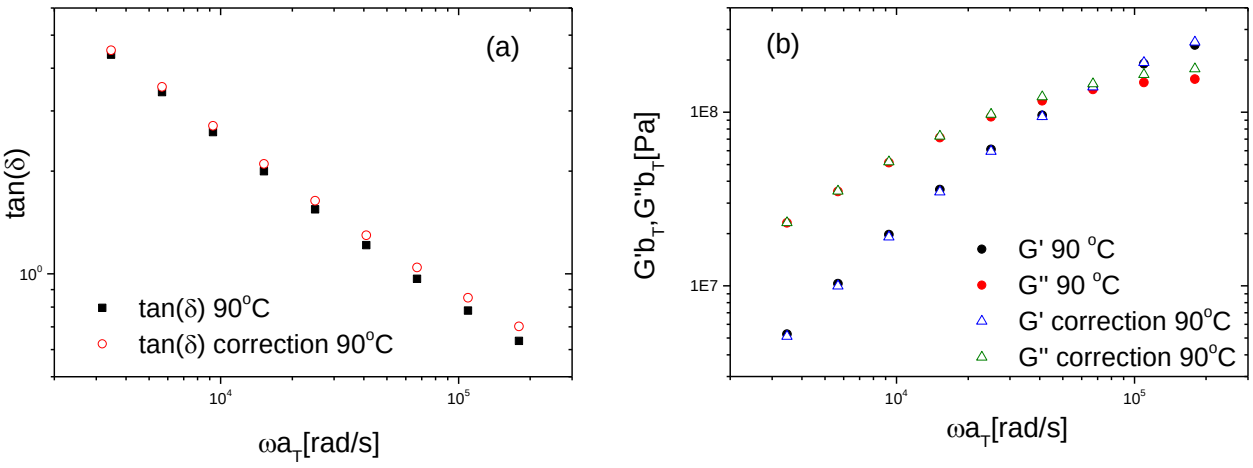

Figure 3.19.(a) Compliance correction for tan(δ), (b) compliance correction for G' and G'' for sample 6 3k

Figure 3.9 is a representation of the compliance correction, figure 3.9(a) is the compliance correction of the tan(δ) and figure 3.9(b) is the compliance correction of Storage and loss modulus. This procedure was performed for all samples.

Below there is a demonstration of the Time Temperature Superposition (TTS), figure 3.10, where the resulting shifted data form the so-called master curve, figure 3.11.

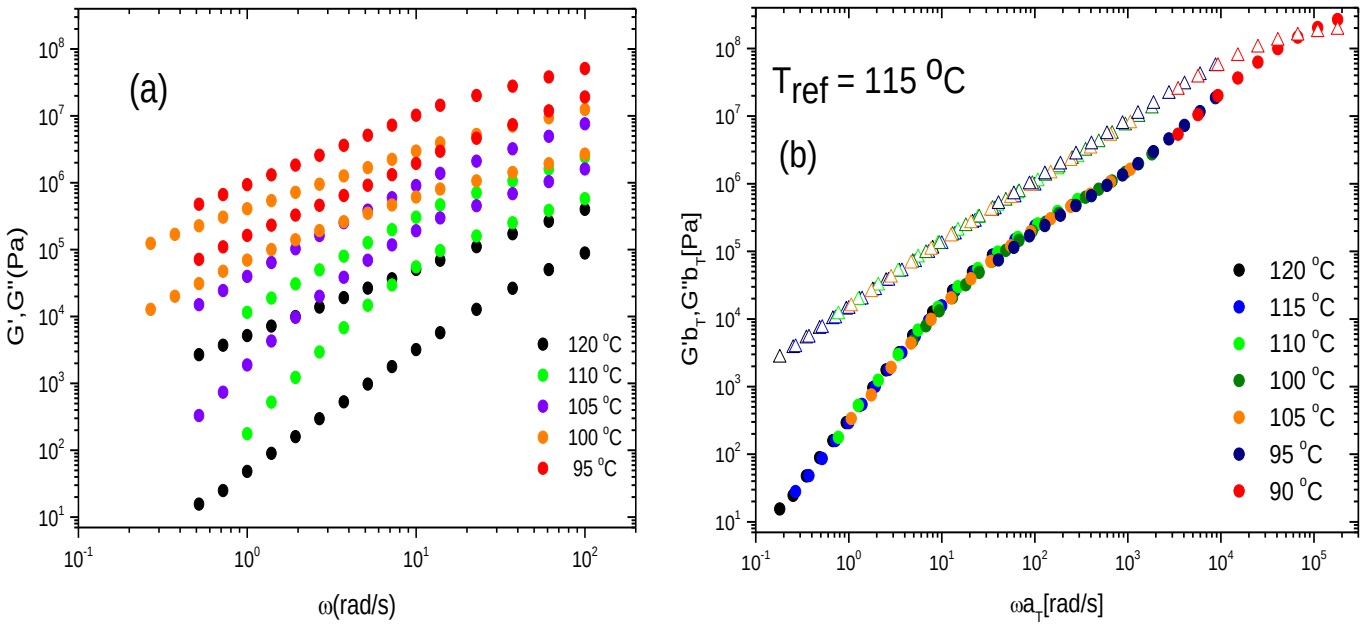

Figure 3.20. (a) Dynamic Frequency Sweep Test for different temperatures for sample 6 Mw=3k and (b) complete master curve.

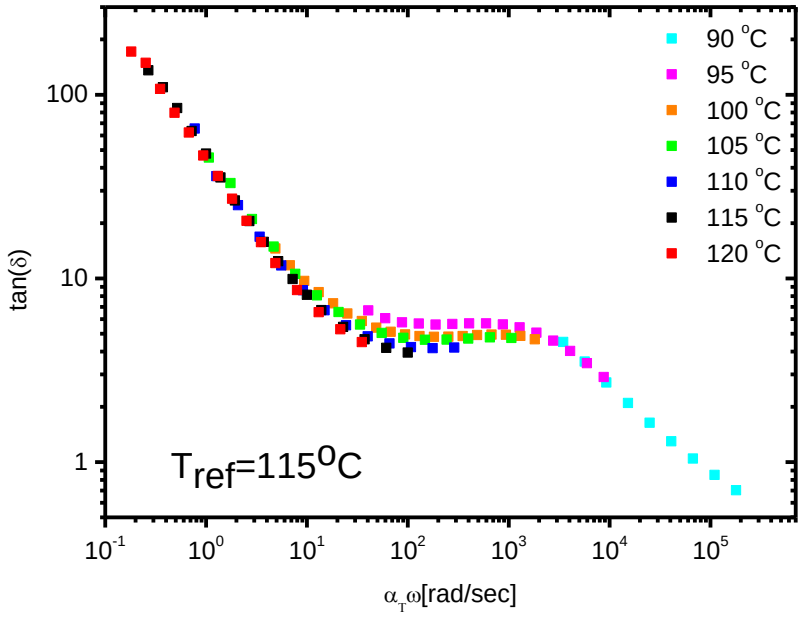

Figure 3.21. Tan(δ) versus frequency for sample 6 3k

For sample comparison, we compared all the samples at the same distance from their glass temperature, Tg+30°C. For this we used the Williams-Landel-Ferry (WLF).

For the horizontal shift factor (frequency axis) α_T:

$$loga_T = -\frac{c_1(T-T_{ref})}{c_2+(T-T_{ref})} \quad (3.6)$$

where c_1 and c_2 are constants (specific for each chemistry). [19]

In this work the selected reference temperature was selected is $T_{ref}=T_g+30^oC$ and the new C_1' and C_2' is given by[23]:

$$C_1' = \frac{C_1 C_2}{C_2+\left(T'_{ref}-T_{ref}\right)} \quad (3.7) \quad \text{and} \quad C_2' = C_2 + \left(T'_{ref} - T_{ref}\right) \quad (3.8)$$

3.2 Relaxation times

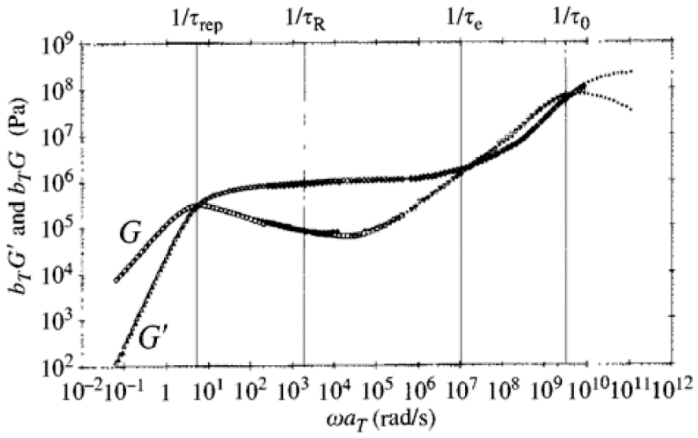

Figure 3.22.Master curve at 25 C from oscillatory shear data at six temperatures for a 1,4-polybutadiene sample with Mw=130000 g mol^{-1}. Figure from R.H. Colby, L.J. Fetters and W.W. Graessley, Macromolecules 20.226(1987)

The relaxation times shown in the figure 3.12 above are the τ_{rep} (also can be referred to as τ_D) which is the reptation or disengagement time, τ_R which is the Rouse relaxation time where $\tau_R=\tau_e*Z^2$ and Z is the number of entanglements. In addition, τ_e is the Rouse time of an entanglement segment (marking the onset of the entanglements regime), finally τ_o is the relaxation time of Kuhn monomer.[6]

3.3 Step Rate Test

During the step rate tests the applied continuous shear rate was held constant throughout the measurement, and the transient stress (known as shear stress growth function) and viscosity (known as shear stress growth coefficient) values was measured over a set period of time. After the selected measuring period the shear rate was set to zero and we monitored the relaxation of the sample for at least 5 to 10 minutes. In the figure 3.13 below the dashed blue line is the end of the application of the shear rate and the start of the relaxation time of the sample.

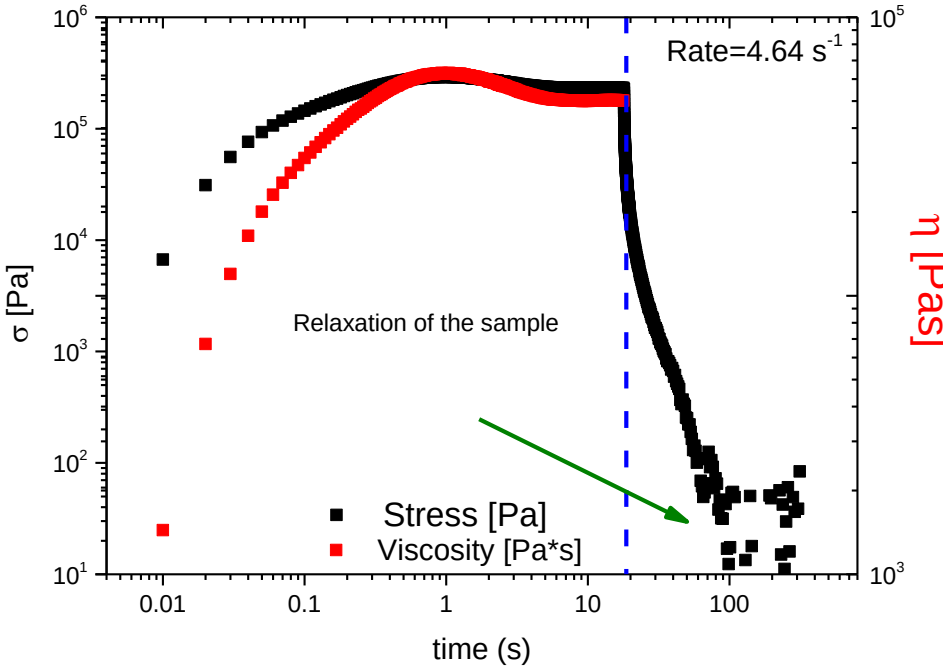

Figure 3.23.Step rate test for sample 3 16k at rate 4.64 s^{-1}

To compare the non-linear responses of different samples/temperatures, we used the Weissenberg Number (W_i) for each specific sample. The Weissenberg Number is a dimensionless number used in the study of viscoelastic flows and is given by the equation:

$$W_i=\frac{elastic\ forces}{viscous\ forces}=\tau\dot{\gamma} \quad (3.9)$$

Here, τ is the characteristic time, for instance in this work we used Rouse time τ_R [24] .

3.4 Cox-Merz Rule

The empirical Cox-Merz rule states that the shear-rate dependent steady-state viscosity equals the frequency dependent complex viscosity, setting equivalence between shear rate and angular frequency ω.[25,26]

$$\eta(\dot{\gamma}) = \eta^*(\omega) \text{ when } \dot{\gamma}=\omega \quad (3.10)$$

Where η^* is the complex viscosity and is calculated through the ratio of the complex modulus (G*) over the frequency (ω) and

$$G^*=\sqrt{(G')^2+(G')^2} \quad (3.11)$$

The Cox-Merx rule has been validated for monodisperse linear polymeric melts.

3.5 Molecular Models for linear Viscoelasticity

3.5.1 Unentangled polymers

The memory function of the Rouse model for a polymer chain with molar mass M is

$$f_{Rouse}(t,M)=\sum_{p=1}^{\infty}\exp\left(\frac{-p^2t}{\tau_R(M)}\right) \quad (3.12)$$

By using the approach adopted by van Ruymbeke[27] *the* Rouse time can be expressed as

$$\tau_{Rouse}(M)=KM^2 \quad (3.13)$$

where K is a material coefficient which scales as $\frac{\tau_e(T)}{M_e^2}$, M_e is the Kuhn molar mass of an entanglement segment, and τ_e is the relaxation time of entanglement strand. As τ_e depends on the temperature, K is a temperature dependent coefficient.

The stress relaxation modulus G (t, M) for unentangled polymers is expressed as

$$G(t,M) = \sum_{M_{min}}^{M_{max}} \frac{\rho RT}{M} f_{Rouse}(t,M) w(M) \quad (3.14)$$

Van Ruymbeke [27] reported K = 2×10^{-12} s $(mol/g)^2$ for entangled polystyrenes at T_{PS} = 170 °C. . In the present case, K takes the value of ~ 2×10^{-9} s $(mol/g)^2$ to obtain the best fit of the observed data. Some considerations on the K coefficient follow. The experimental τ_e is 0.002s at 150 °C [21,28] and the WLF constants at the same temperature are C_1 = 7.2 and C_2 = 103K. It follows that $\tau_e(170\,°C) = 0.00013$ s, and therefore $M_e = \sqrt{\frac{\tau_e}{K}} = \sqrt{\frac{0.00013}{2\times10^{-12}}} \cong 8.2$ kg/mol. The latter seems to underestimate the experimental M_e by a factor of about 2 For S11(entangled see table 1), $\tau_e(131\,°C) = 0.085$ s. The ratio between the entanglement time, which also reflects the ratio of the K coefficients, at the two above-reported temperatures, is $\frac{\tau_e\,(131°C\,)}{\tau_e\,(170°C)} \cong 654$. This value is not very far from the ratio $\frac{K\,(131°C\,)}{K\,(170°C)} \cong 1000$ found as a best fit of the observed data.

3.5.2 Entangled polymers

The relaxation dynamics of entangled polymers are predicted by the sum of three relaxation modes: 1) Fast Rouse, 2) Longitudinal modes, and 3) Reptation.

The fast Rouse relaxation modes can be expressed by equation 3.15 below, where M/M_e is the number of entanglement strands per chain.

$$f_{F,Rouse}(t,T,M) = \frac{M_e}{M} \sum_{p=M/M_e}^{M} exp\left(-\frac{2p^2 t}{\tau_R(T,M)}\right) \quad (3.15)$$

Importantly, here we consider $\tau_R(M) = \tau_e M^2/M_e^2$, with τ_e being the experimental value and M_e equal to 17.5 kg/mol.

The longitudinal mode function (along the confining tube) can be described as Rouse modes. It was analyzed by Likhtman, Milner and McLeish[29,30] and originates from the fact that because different tube segments before deformation are oriented differently, they also stretch differently, hence, redistribution of monomers along the tube takes place after the deformation. It was shown[30] that these relaxation modes contribute to the relaxation of 1/5 of the total stress stored in the tube.

$$f_{Long}(t, M) = \frac{M_e}{5M} \sum_{p=1}^{M/M_e - 1} exp\left(-\frac{2p^2 t}{\tau_R(M)}\right) \quad (3.16)$$

Both fast Rouse and longitudinal modes are active for relaxation times up to the Rouse time of the chain. Note that the glassy dynamics at high frequencies is not considered in the present work.

The Rouse contribution to the stress relaxation modulus $G_{Rouse}(t, M)$ for entangled polymers writes

$$G_{Rouse}(t, M) = \sum_{M_{min}}^{M_{max}} \frac{\rho RT}{M_e} [f_{F,Rouse}(t, M) + f_{Long}(t, M)] w(M) \quad (3.17)$$

where ρ is the polymer density, R is the universal gas constant, and $w(M) = dW(M)/dlog(M)$ with the weight fraction of all chains having a molar mass below M.

The entanglement relaxation function can be expressed by the time-dependent diffusion model derived by des Cloizeaux[31].

$$F_{TDD}(t, M) = \frac{\pi}{8} \sum_{p\ odd} \frac{1}{p^2} \exp\left(-p^2 U(t)\right) \quad (3.18)$$

The function U(t) writes as

$$U(t, M) = \frac{t}{\tau_{rep}} + \frac{M_e}{M} g\left[\frac{tM}{\tau_{rep} M_e}\right] \quad (3.19)$$

and

$$g(y) = \sum_{n=1}^{\infty} \frac{1-\exp(-n^2 y)}{n^2} \quad (3.20)$$

The reptation time (which encompasses non-reptative mechanisms as well) is defined as

$$\tau_{rep}(M) = \tau_e \left(\frac{M}{M_e}\right)^{3.4} \quad (3.21)$$

The first term of equation 3.19 identifies the relaxation by reptation, whereas the second term represents the contributions of contour length fluctuations.

The reptation contribution to the total stress relaxation modulus can be expressed as follows:

$$G_{rep}(t, M) = \frac{\rho RT}{M_e} \sum_{M_e}^{\infty} [F_{TDD}(t, M)]^{\beta} w(M) \quad (3.22)$$

where the exponent β is set to a value of 2, according to the double reptation concept[32]. It is now possible to evaluate the total stress relaxation modulus by summing equations 3.17 and 3.21:

$$G(t, M) = G_{Rouse}(t, M) + G_{rep}(t, M) \quad (3.23)$$

For samples (like SB2) which are at the limit between an entangled and an unentangled regime, a different approach to fit the data was used. Indeed, using the unentangled approach, faster dynamics are obtained. Conversely, by using the entangled model, dynamics are overestimated. To this end, the total stress relaxation modulus was calculated as the sum between the fraction of the short chains, multiplied by the effective unentangled modulus, and the fraction of the long chains, multiplied by the entangled modulus.

$$G(t, M) = \phi_{unentangled} G_{unentangled}(t, M) + (-\phi_{unentangled}) G_{entangled}(t, M) \quad (3.24)$$

4. Results and Discussion

4.1 Linear Regime

For the oscillatory measurements the temperature was ranging from 90°C to 160°C. At higher temperatures the materials exhibit a liquid-like behavior whereas at the lowest temperatures they exhibit a solid-like behavior. A DSS (Dynamic Strain Sweep) test was performed in order the determine the linear viscoelastic regime, at ω=100rad/s and a strain amplitude ranging between 0.1% and 12 %. The DSS was followed by the DTS (Dynamic Time Sweep) at 10 rad/s in the LVE regime. The duration of the test depended on the sample and the temperature and was at least 45 minutes. Finally, linear viscoelastic (LVE) spectra were obtained by means of DFS (Dynamic Frequency Sweep) tests. This procedure was followed for all the samples and at each temperature. The range of the temperatures depended on the sample. Typically, the full linear viscoelastic spectrum (master curve), from the glassy regime to the terminal flow was attained by creating master curves using TTS at a reference temperature is T_g+30°C.

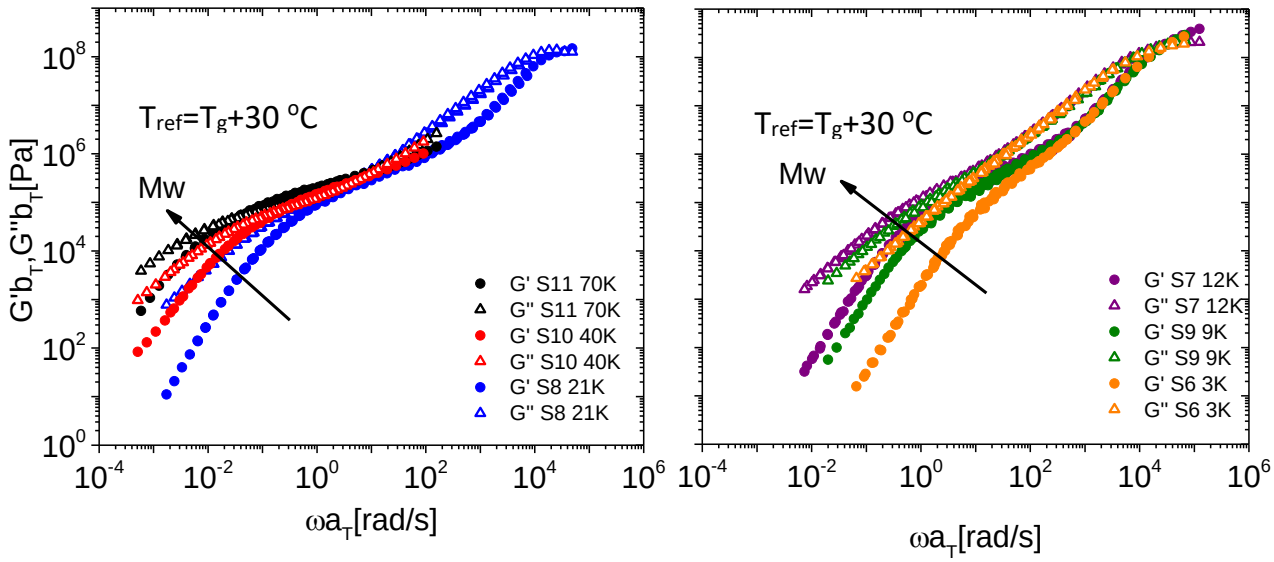

Figure 4.1. Master curves of G'(closed symbols) and G''(open symbols) for linear individual PS samples at a temperature of T_{ref}=Tg+30 C

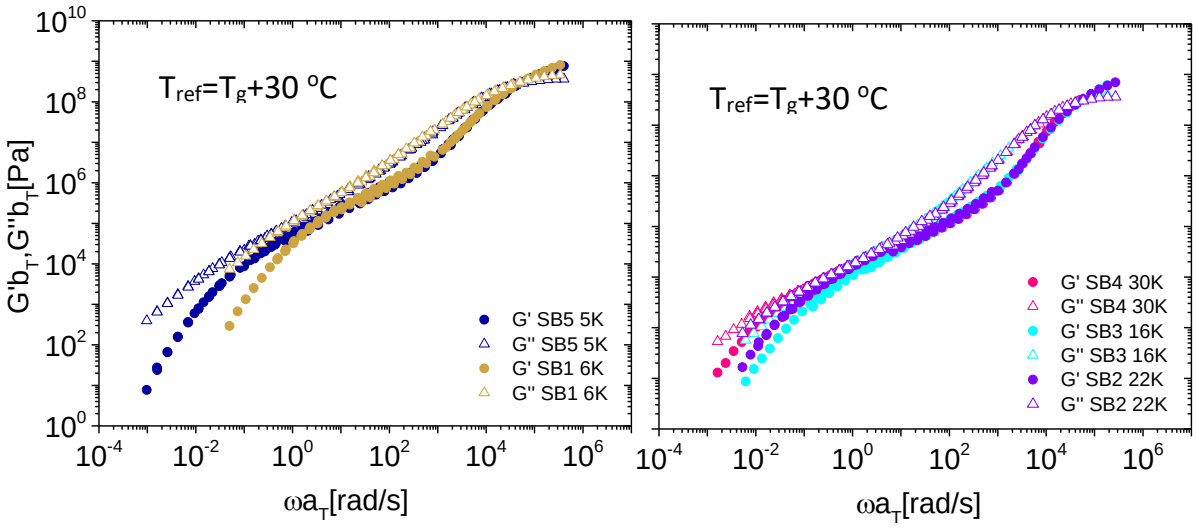

Figure 4.2. Master curves of G'(closed symbols) and G''(open symbols) for linear blends PS samples at a temperature of T_{ref}=Tg+30 C

S11 (70k) and S10 (40k) have a rubbery plateau region since the molecular weight is higher than the entanglement molecular weight of M_e=17kg/mol for polystyrene. On the other hand, there is no plateau for the rest of the samples as shown in the figures 4.1 and 4.2 as the molecular weight of the samples is smaller than the entanglement molecular weight for polystyrene. The master curves shown in Figure 4.2 demonstrate a primarily viscous response to the deformation, as G'' remains higher than G' at nearly all frequencies. In figure 4.3 below the vertical shift factor b_T and the horizontal shift factor a_T for all the samples are depicted, at a common reference temperature of 130 °C.

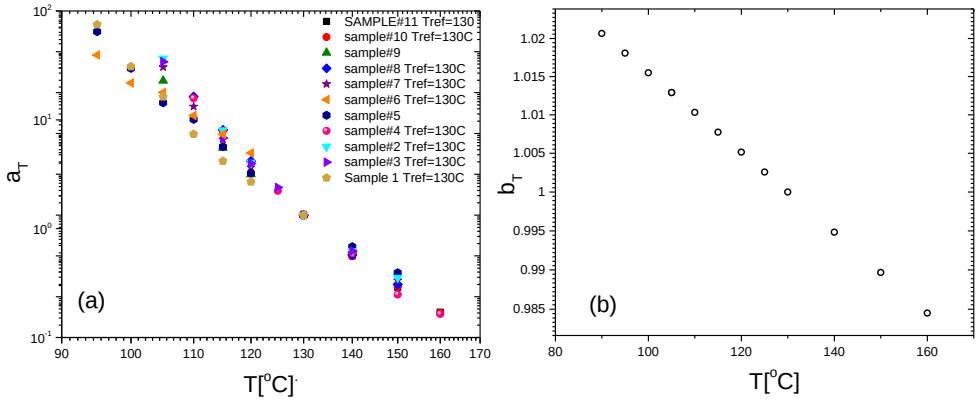

Figure 4.3 (a) Horizontal shift factors and (b) vertical shift factors at a common temperature of 130 C

A sensitive indicator of the quality of the LVE master curve is the Van Gurp-Palmen plot, which presents the phase angle (δ) versus the complex modulus G*. The overlapped data validity of time temperature superposition principle[18] for the specific polymeric systems. In the figure 4.4 below the blue dashed line shows the entanglement rubbery plateau at the value δ_{min} which decreases as the molecular weight increases and the material exhibits more extended elastic response, always with the same rubbery plateau modulus. On the other hand, for the unentangled linear polymers δ_{min} is related with steady state recoverable compliance Js. As the molecular weight decreases the minimum appears at a higher modulus since the compliance can be expressed as inverse modulus and the value of the phase angle increases (for instance S6 3k and the system is completely liquid-like).

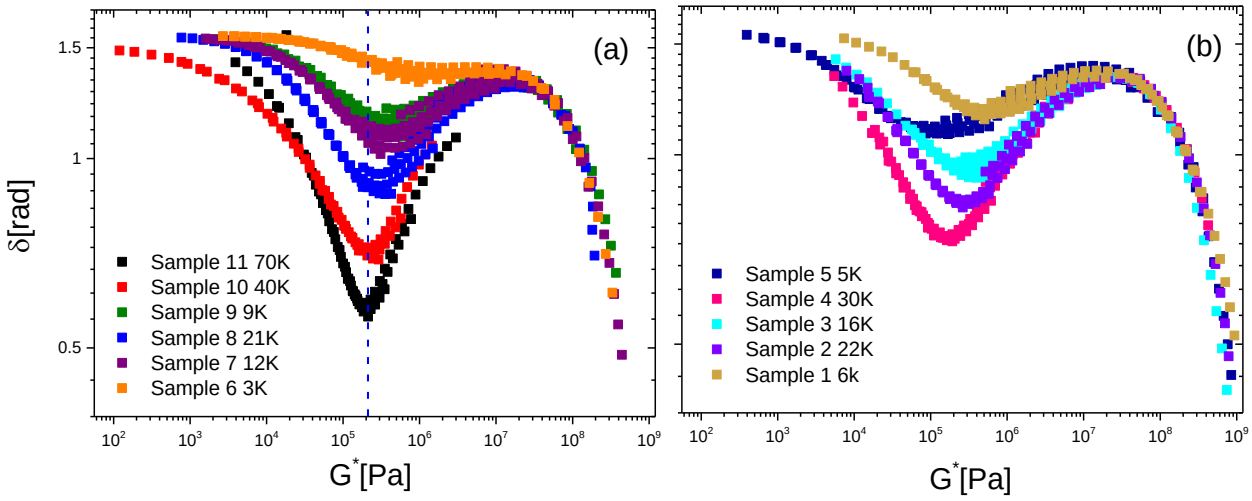

Figure 4.4 Van Gurp-Palmen plot for individual samples (a) and blends (b).

The figure 4.5 below depicts the complex viscosity master curves of the pure (single component) polystyrenes and as well as their blends. At high frequencies the curves overlap because of the same segmental behavior. All individual samples have a clear rubbery plateau, whereas this is not the case for the blends. We can observe that the samples with the higher molecular weight have larger complex viscosity, as expected. In the high frequency region above the plateau, the viscosity scaling with frequency (S11 and S10) conforms to the Rouse prediction of $\eta^* \sim \omega^{-1/2}$. On the other

hand, the power-law exponent for the unentangled polymers ranges from -0.32 to -0.37. This scaling is consistent with the Zimm model[33], $\eta^* \sim \omega^{-1/3}$.

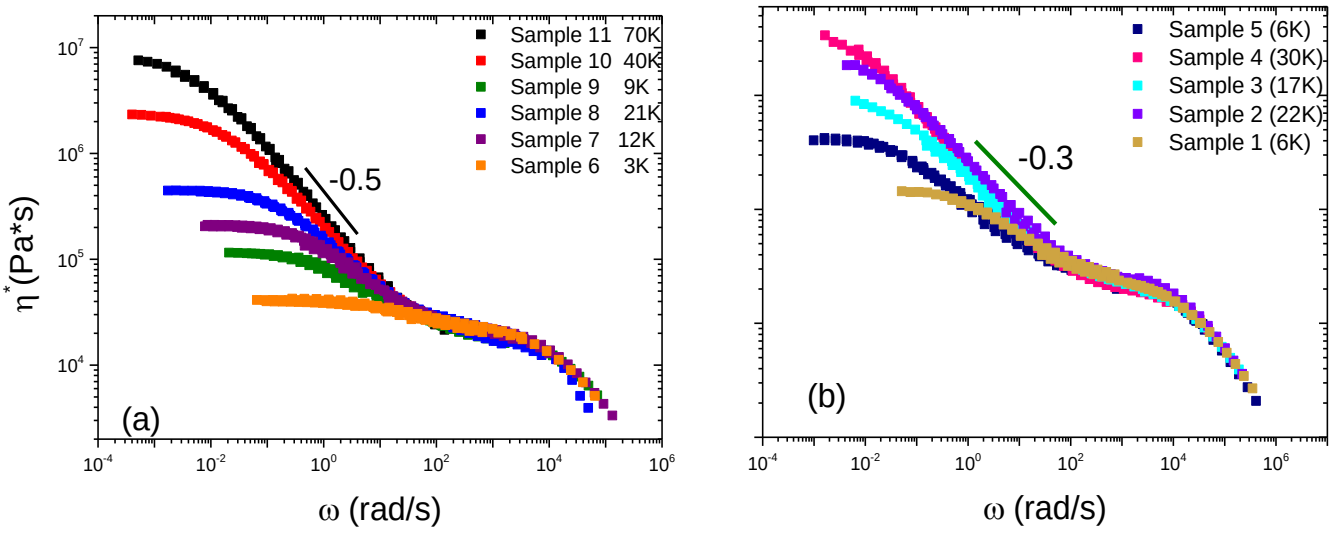

Figure 4.5. (a) Complex viscosity versus frequency at T_{ref}=Tg+30 C for individual samples and (b) blends. A black line with a slope of -0.5 is shown in (a) plot and a green line with a slope of -0.3 in (b) plot

We also calculated the zero-shear viscosity. The zero-shear-rate viscosity (often called zero-shear viscosity) is a widely used and fundamental descriptor of the flow resistance of a fluid. It is important for characterizing rheological response at low stress and for examining the influence of molecular architecture on resistance to flow. The zero-shear-rate viscosity is a limiting value that cannot be measured directly; rather, it must be estimated by extrapolation. The value determined by extrapolation will depend on the viscosity model used, and the range and quality of the data used for the extrapolation and the error can be large.[34]

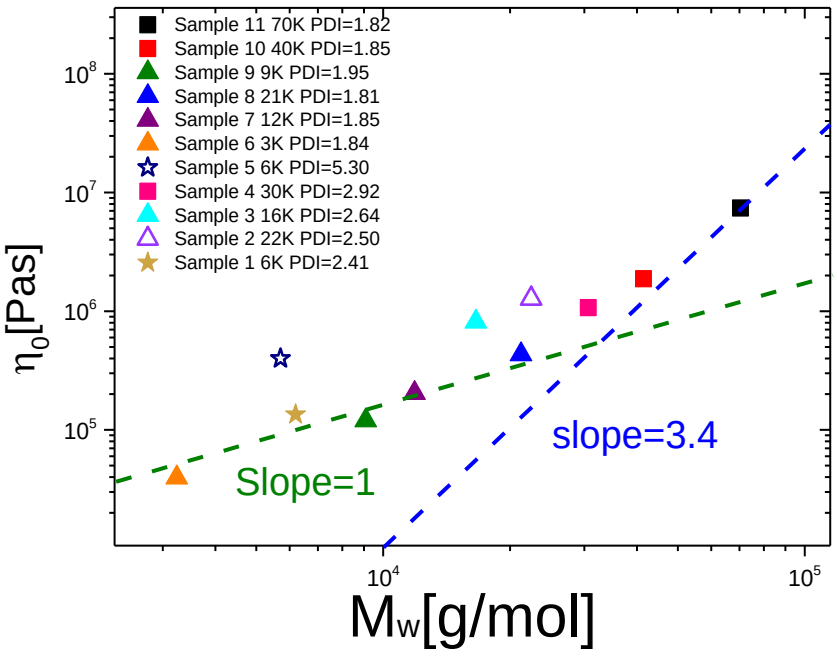

Figure 4.6. Zero shear viscosity versus the molecular weight at T_{ref}=Tg+30 C for all the samples

From the literature[10] we know that zero-shear viscosity dependence on Mw for linear polymer chains follows a trend described by a function like: $\eta_0=KM_w^{\alpha}$ where alpha is 3.4 for $M_w>M_c$ for monodisperse systems. From the figure 4.6 above we can see that the blends with large polydispersity significantly deviate from the predicted slopes. This is not something that we didn't expect since as Graessley showed[35], the Doi Edwards tube model predicted a strong dependence of zero shear viscosity on MWD but for polydisperse systems it is essential to account for constraint release. Over the years there have been numerous attempts to determine the effect of polydispersity on η_0 but there is not yet a clear result. In the figure 4.6 above we can observe the two stars symbols (open and closed), these samples have the same average molecular weight but different molecular weight distributions and polydispersity.

Polymer molecular weight is defined as a distribution rather than a specific number because polymerization occurs in such a way to produce different chain lengths. Weight average molecular weight (M_W) and number average molecular weight (M_N) are some of the ways we can

characterize the polymer molar mass[36]. The Gel permeation chromatography (GPC) method is used widely to measure molecular weights of linear polymers. High-quality GPC data contains detailed information on many aspects of the polymer's molecular weight distribution (MWD)[11]. Gel permeation chromatography (GPC) is a type of size-exclusion chromatography (SEC), that separates analytes on the basis of size. The separation is based on the elusion time of the different sizes. The relation between these times and sizes is expressed in the figure 4.7 as distribution. Figure 4.7 exhibits the MWD of SB1 and SB5 and the dashed line represents the average Mn of the samples (Table 1). In order to quantify the polydispersity of samples SB5 and SB1 with the same Mw average, we used a ratio of long chains over short chains. To do so, we divide the MWD in two areas. Area 2 is considered to have the short chains and area 1 the long ones. With the use of peak analysis for these samples, we calculated the area (1) above the average molecular weight (dashed line) and the area (2) below for both samples.

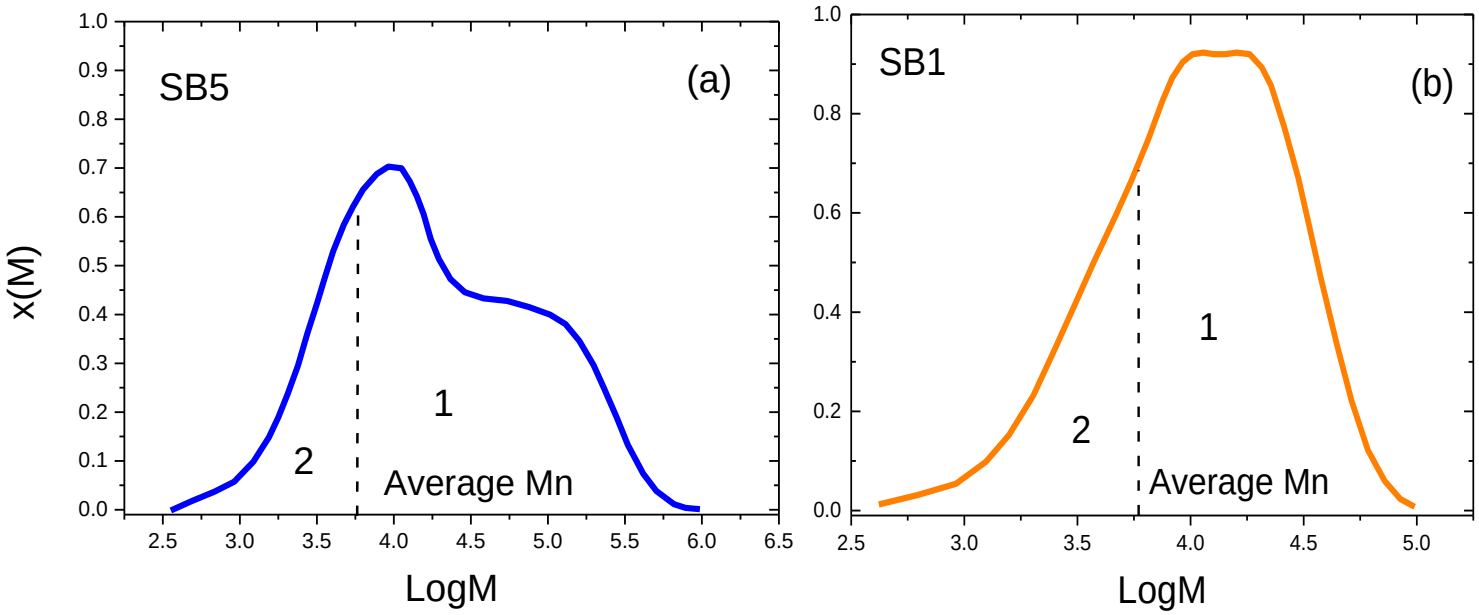

Figure 4.7. Molecular weight distribution of SB5 (a) and SB1 (b).

pFor SB5 the area 1 shown in figure 4.7(a) was calculated with the use of peak analysis and was estimated to be around 0.853 whereas the area 2 shown in the same figure was estimated to be 0.265. The ratio of area 1 by area 2 for SB5 is 3.21. The same procedure was followed for SB1 shown in figure 4.7(b) and the ratio of the area 2 by area 1 for SB1 is 2.39. The results of the calculations are shown in table 2 bellow. Based on this we conclude that SB5 has more long chains in comparison to SB1 since the ratio of SB5 is larger than SB1. This phenomenon led to SB5 having an increase in the viscosity in comparison to SB1, as we can see in the figure 4.6.

Table 2: Calculation of different areas in the MWDs reported in figure 4.7.

	SB5	**SB1**
Area 1	0.853	0.708
Area 2	0.265	0.296
$\frac{\boldsymbol{Area\ 1}}{\boldsymbol{Area\ 2}}$	3.21	2.39

Finally, we present the comparison between the linear viscoelastic experiments and the theoretical models, in terms of stress relaxation modulus, G(t), as a function of time. The challenge here was to account for the polydispersity of the samples and the complex MWD obtained by means of the blends (Table 1 in materials and methods). As reported in the previous chapter, we adopted two molecular models, one describing the unentangled polymers (Rouse) and one for the entangled systems (double Reptation). Each model uses as an input the experimental molecular weight distribution. The Glassy modes were excluded in both models. As shown in the materials and methods chapter in Table 1 S11, S10 and SB4 are entangled whereas the rest of the samples in this work are unentangled. For the modeling we included the experimental MWD, the entangle polymers were modelled with the use of double reptation model using equations 3.21 and 3.22 and there are no fitting parameters. We consider $\tau_R(M) = \tau_e M^2/M_e^2$, with τ_e being the experimental value and equal to 0.085 at Tg+30°C, M_e equal to 17.5 kg/mol and β the double

reptation exponent equal to 2. On the other hand, for the unentangled polymers we only had one fitting parameter, K which is a material coefficient taking the value of of ~ $2x10^{-9}$ s (mol/g). This parameter is temperature and chemistry dependent and was found in close agreement with that reported in the literature[27] for polystyrene but at different temperature. The difference in our value of K in comparison to the value from the literature is mostly associated to the difference in τ_e because of the temperature. These samples were a good model system to test the mechanical models with complex MWDs and as seen in figure 4.8 it is possible to use such models to describe the dynamics with blends with complex distribution. For SB5 the model seems to predict a high-M mode which is due to the tail of the MWD, experiments in higher temperatures in order to extend the low frequency region may be useful and performed in the future. SB2 which is at the limit between an entangled and an unentangled regime, a different approach to fit the data was used. We used equation 3.24 and the mass fraction for equation 3.22 was taken from table 1.

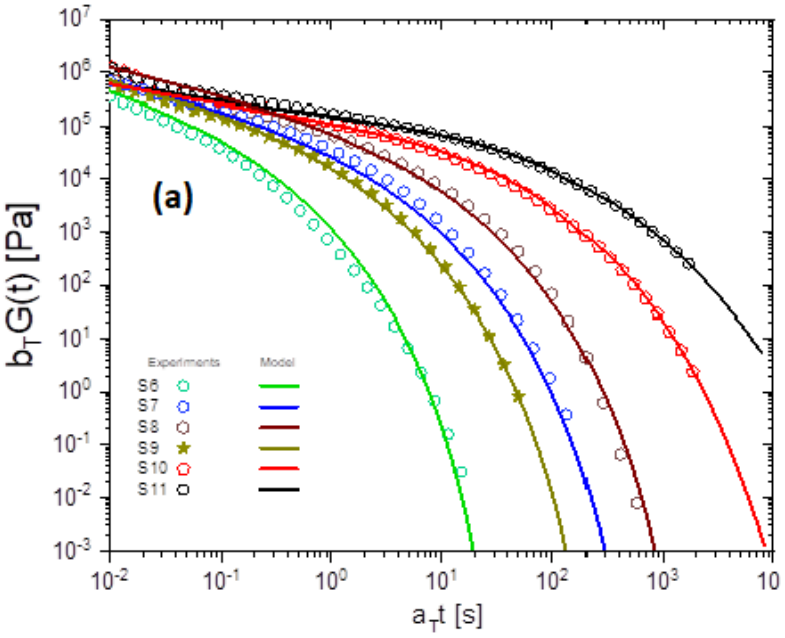

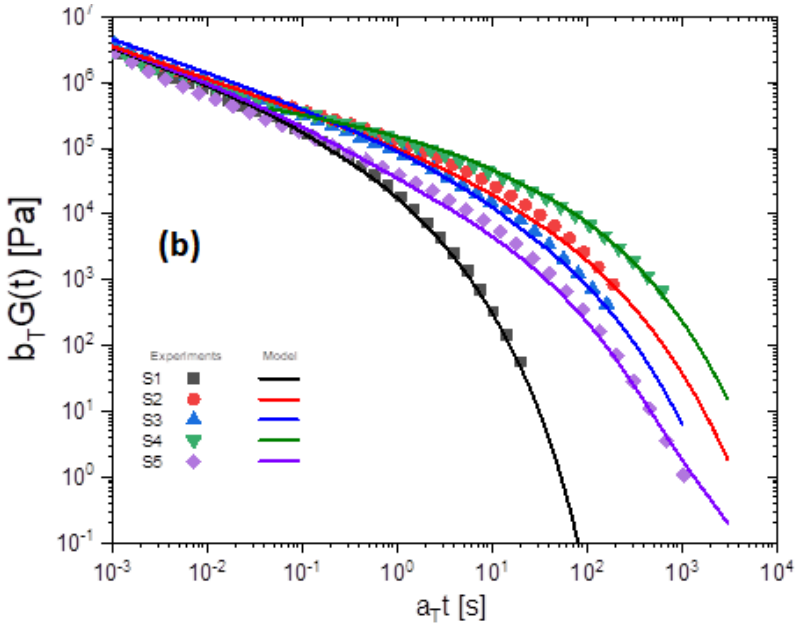

Figure 4.8. Shifted stress relaxation modulus as a function of shifted time. Symbols and lines represent observed data and theoretical predictions, respectively. The panel (A) refer to the individual polymers, whereas panel (B) to the blends

4.2 Nonlinear Regime

With the use of CPP geometry we performed nonlinear shear measurements for 3 entangled polystyrene samples, single components S11 70k, S10 40k and blend SB4, as well as 4 unentangled samples ranging from 12k to 22k. For each sample we performed start-up of shear rate tests at different shear rates and a temperature of choice, based on the LVE. The selection criterion was for the sample to exhibit viscoelastic behavior and Weissenberg number exceeding the value of 1. Figure *4.9* represent the shear data expressed by the transient shear viscosity over the time at various shear rates. The navy, red, blue and purple lines are the transient viscosity and the black lines are the linear viscoelastic envelope obtained by dynamic frequency sweep tests.

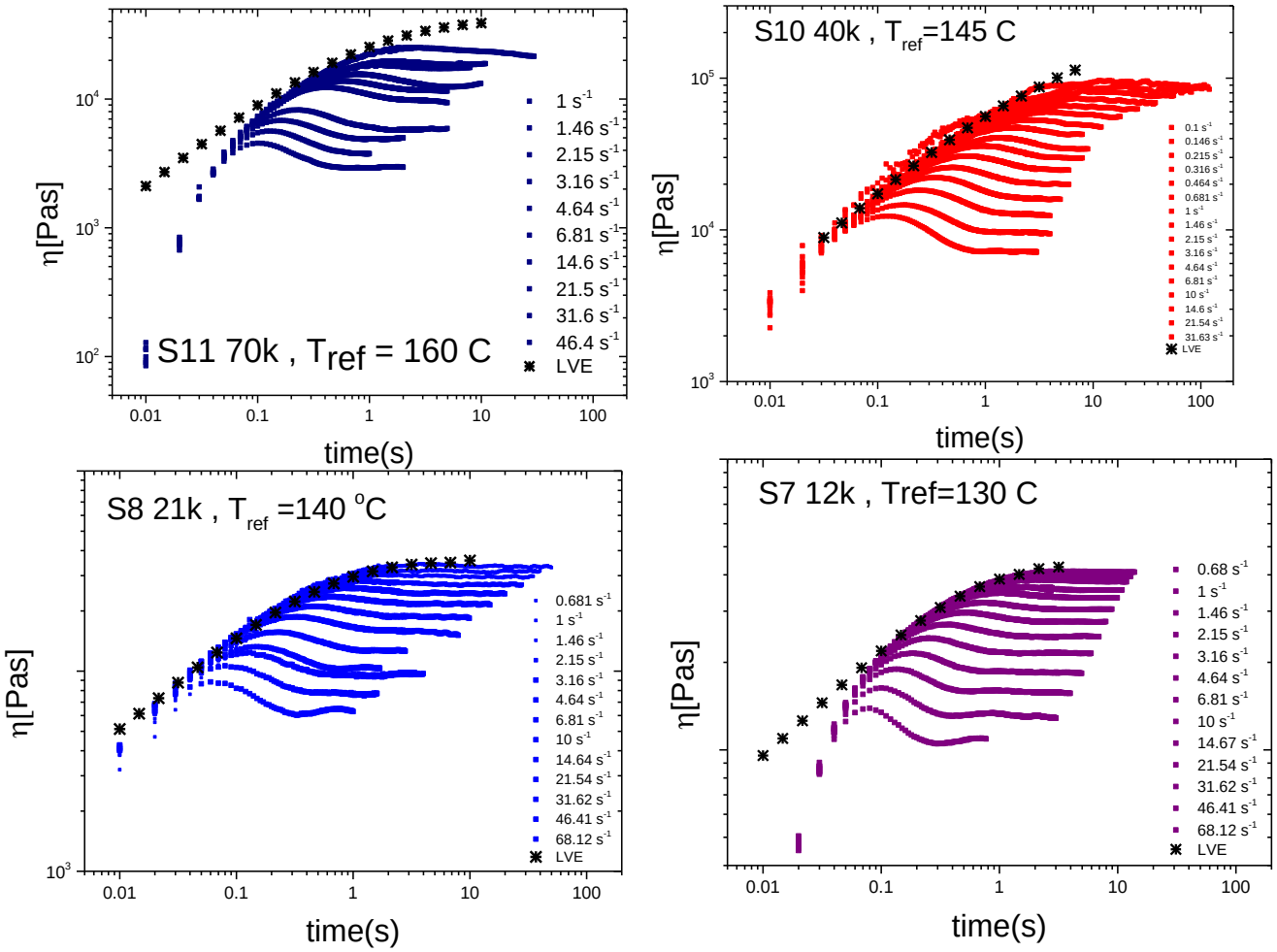

Figure 4.9. Transient shear viscosity at different shear rates for the individual samples S11 70k, S10 40k, S8 21k, S7 12k. The star symbols are LVE envelopes.

At the lowest shear rates, the response of the polymers is linear, as confirmed by the coincidence of the steady shear data with the LVE envelope, extracted from the dynamic oscillatory data. As the shear rate increases the transient viscosity (shear stress growth coefficient) exhibits an overshoot which becomes more pronounced,[37] before reaching the steady-state value. At lower molecular weights we can also observe an undershoot[14] after the overshoot and before the steady state. This is clearly evident at the highest rate of S8 and S7. We can also note that all four samples obey the empirical Cox-Merz rule as shown in figure 4.10.

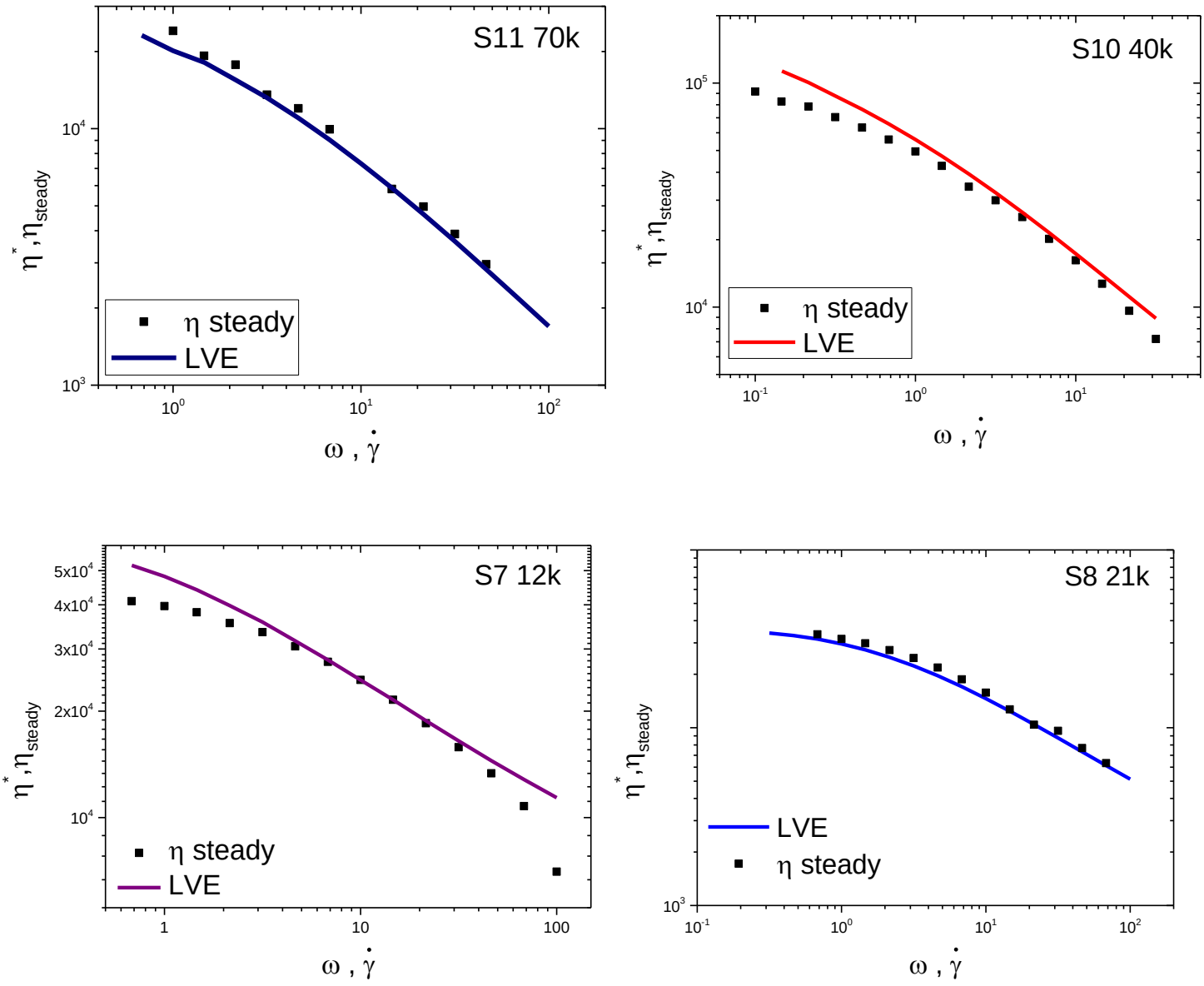

Figure 4.10. Cox-Mertz rule for samples 11 70k, S10 40k, S8 21k, S7 12k

Closer inspection of figure 4.10 suggests that at low frequencies we there is a small deviation of the steady data from the respective LVE data. However, the deviation between the two data sets is below 20% (with respect to the LVE data), and if we take into consideration experimental uncertainties (including alignment of the tools and sample loading), we conclude that this mismatch is minimum.

Similarly, to the individual samples, the blends investigated also exhibit a transient viscosity overshoot as the shear rate increases. As the shear rate increases, we can observe the overshoot more clearly. Figure 4.11 represent the shear data expressed by the transient shear viscosity over the time at various shear rates. The pink, olive and violet lines are the transient viscosity and the black lines are the linear viscoelastic envelope obtained by dynamic frequency sweep tests.

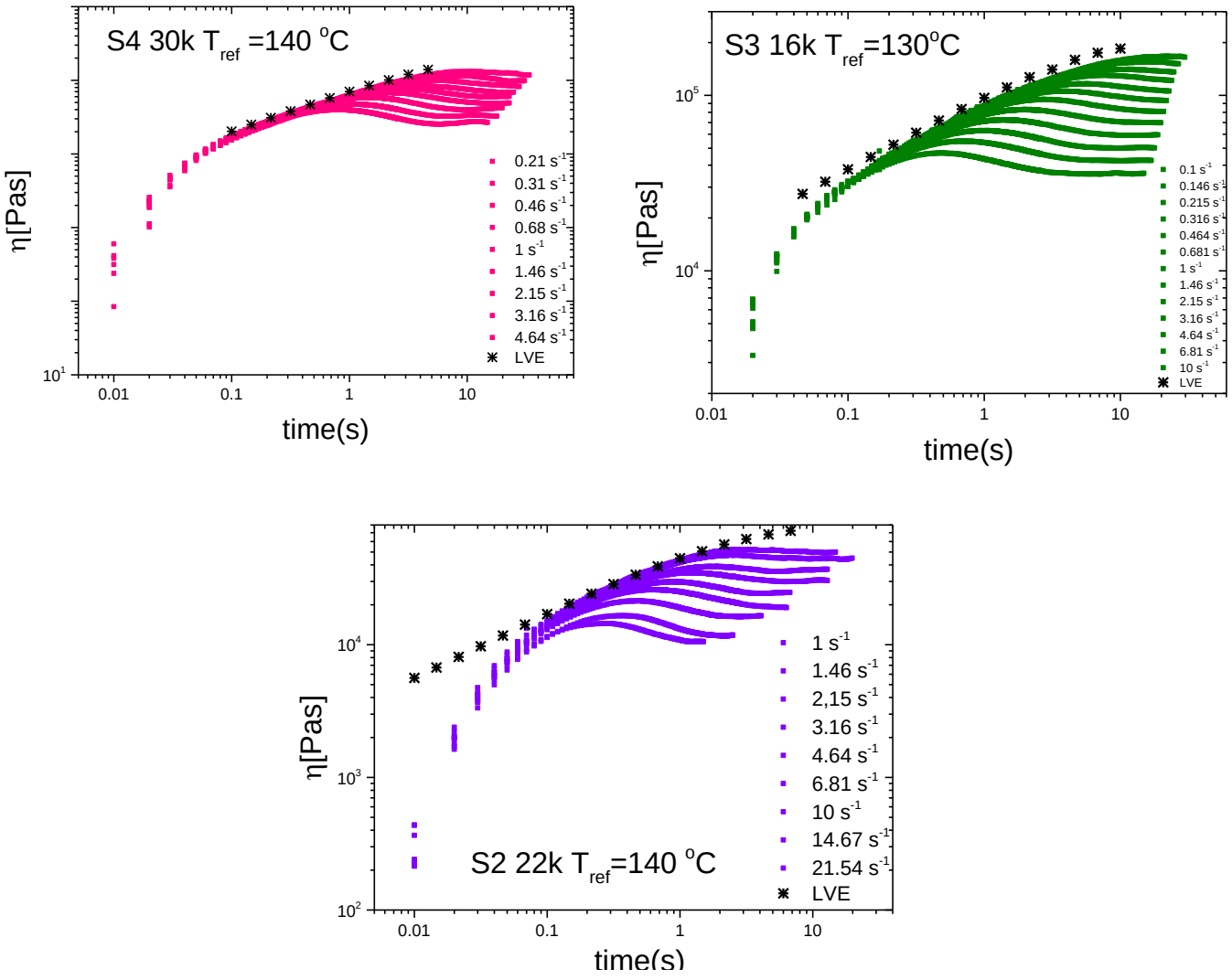

Figure 4.11. Transient shear viscosity at different shear rates for the individual samples S4 30k, S3 16k and S2 22k.The star symbols are LVE envelopes.

The validity of the Cox Mertz rule for all blends is demonstrated in figure 4.12. Here, the data collapse at low frequencies for SB3 and SB4. Whereas a small deviation is observed for SB2. Again, it does not exceed the 20% and is attributed to experimental uncertainties.

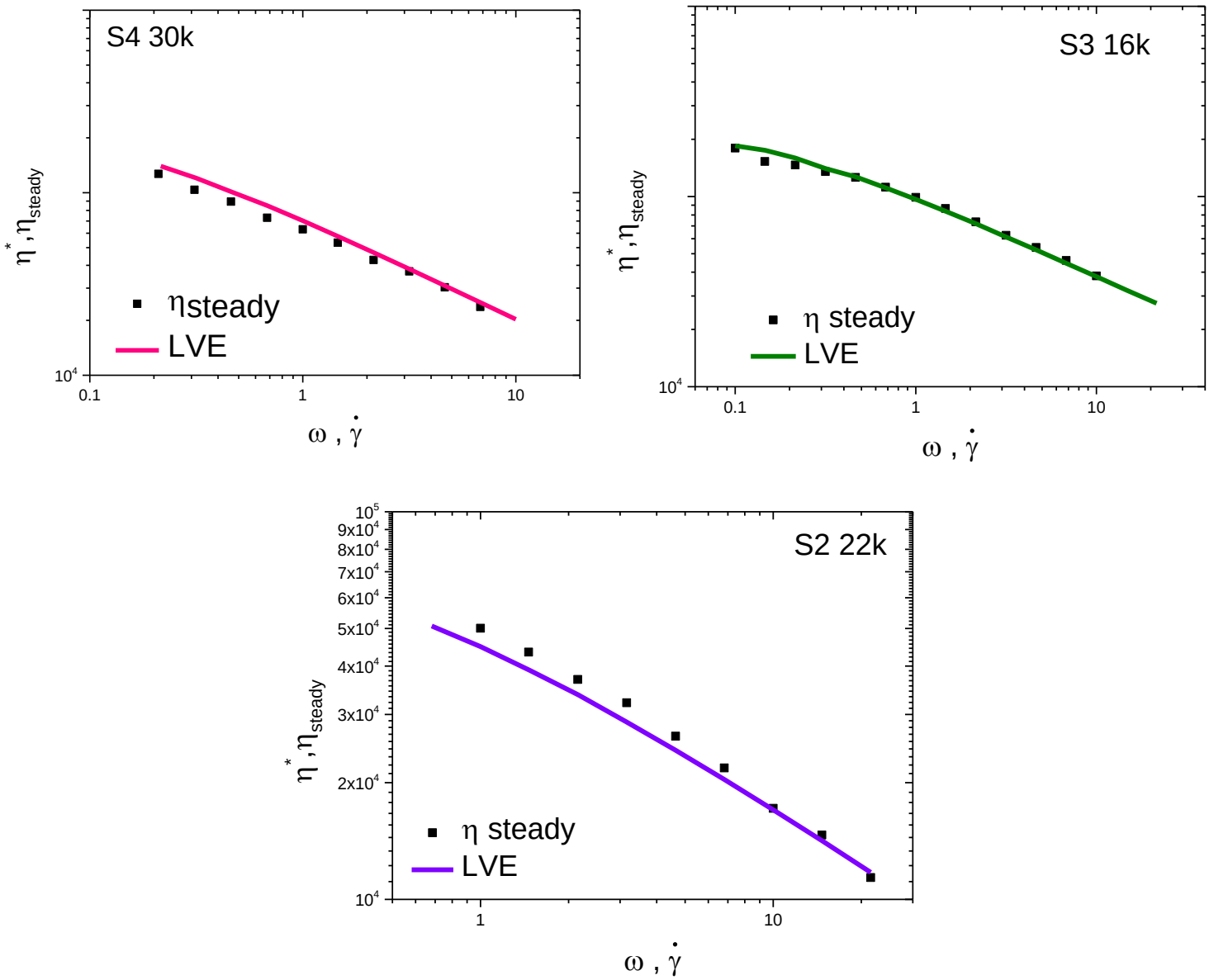

Figure 4.12. Cox-Mertz rule for SB4 30k, SB3 16k and SB2 22k

In order to compare the nonlinear data quantitatively, we analyze them and discuss below the parameters extracted from the transient viscosity signal.

In the figure 4.13 bellow we have plotted the strain at overshoot as a function of the Weissenberg number based on the Rouse time. We observe that for the entangled samples, at low Wi_R values (typically up to 1) S11 70k and S10 40k, the value γ_{max} follows the dashed black line which is the well-known Doi-Edwards value of 2.3[38]. For faster flows where the Wi_R is greater than 1, γ_{max} increases because there is chain stretching. In figure 4.13 the green dashed line is the expectation for monodisperse samples, we observe that S11, S10 and S8 which have a low polydispersity index value follow this slope. Whereas SB4, SB3 and SB2 that have an increased polydispersity index do not follow this slope and seems that their slope has increased.

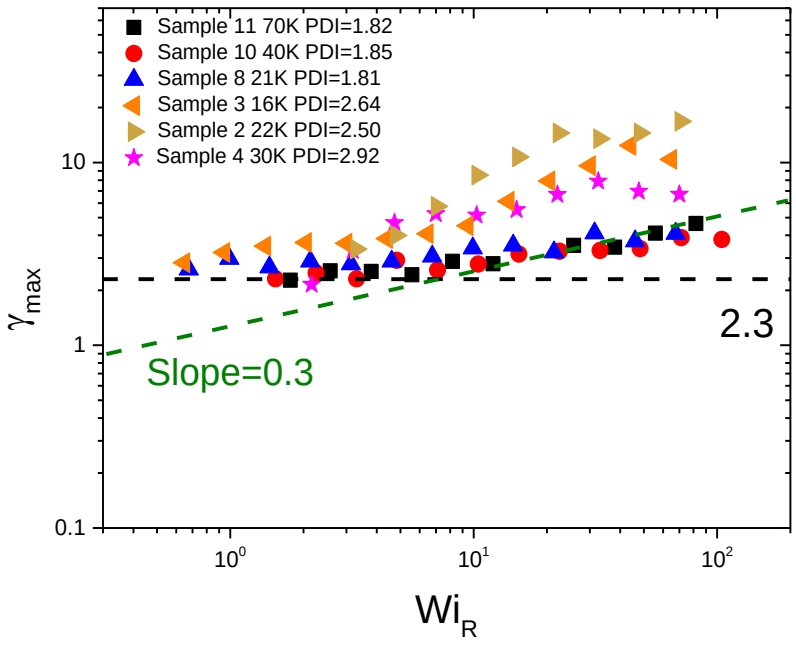

Figure 4.13. Peak strain versus the Rouse Weissenberg number for all samples.

In order quantify the average loss of entanglements at steady state we plot in figure 4.14 the ratio of the value of η_{max} by the η_{steady} versus the Rouse Weissenberg number. For low values of Weissenberg number, the data seems to collapse at the value of 1 (no overshoot) of the ratio η_{max} and η_{steady}. For the entangled systems there is a slight increase with the increasing of the Wi_R with a slope of 0.2[39], whereas for the unentangled systems there is also in increase as the Wi_R increases but with a slope of 0.1 as seem in figure 4.14.

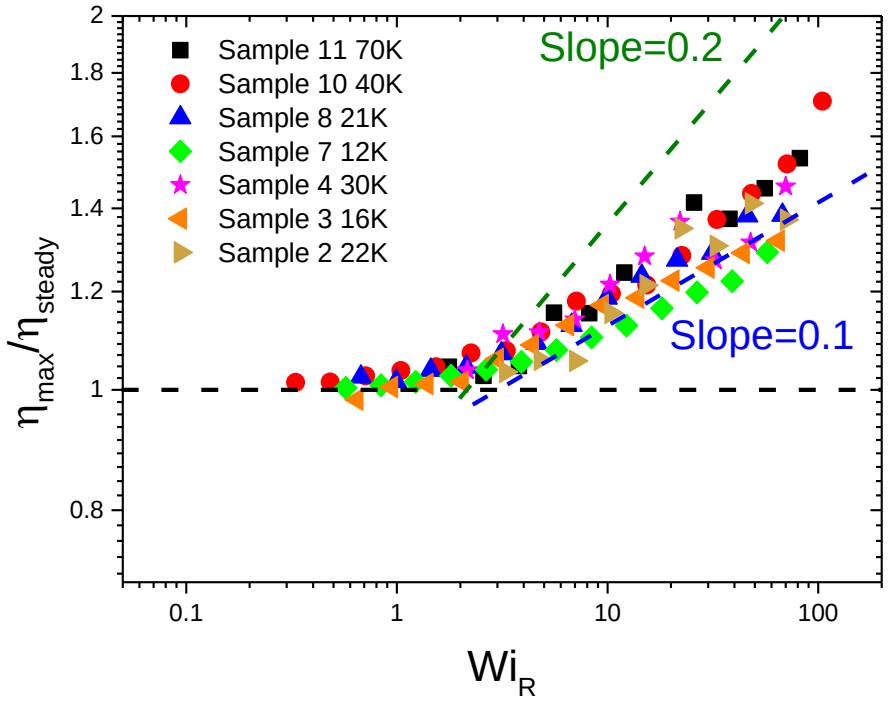

Figure 4.14. Ratio of η_{max} and η_{steady} vs Rouse Weissenberg number. The slope of entangled systems is the green dash line with a slope of 0.2 and for the unentangled a blue dash line of slope 0.1

Next, we then proceeded to calculate the broadness of the viscosity peaks plotted against time for all samples. We calculated this by finding the η_{max} and η_{steady} for every peak and adding their values and then dividing them by 2. By this was we got the full width at half maximum (FWHM). In order to calculate the width of the curve we subtracted the viscosity value η_2 with the viscosity value η_1. This is illustrated in figure 4.15.

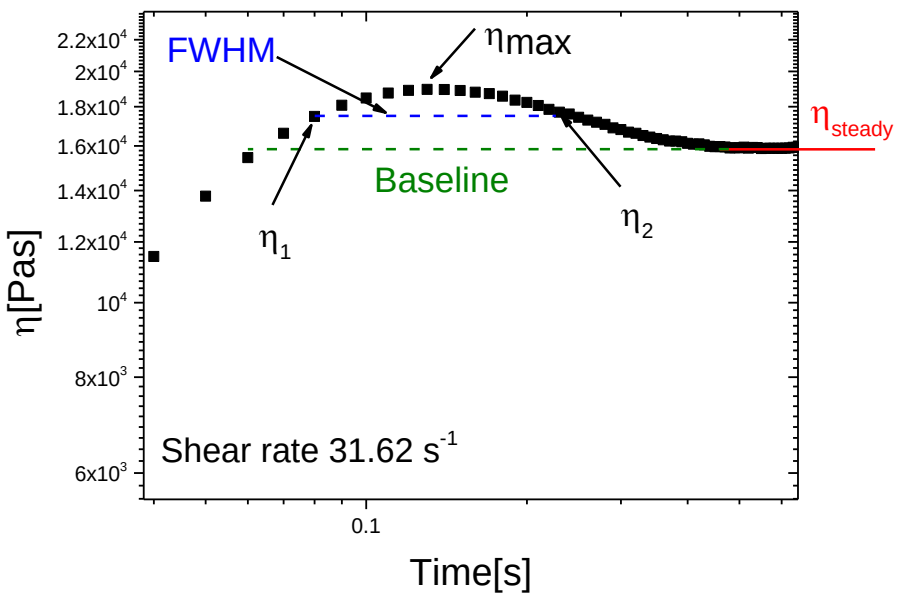

Figure 4.15. Calculation of FWHM. Green dash line is the base line, blue dash line is the FWHM

The FWHM provides information about the process of flow-induced disentanglement and is plotted in figure 4.16 for all the samples as function of the shear rate. We compared our data with a monodisperse entangled sample from the literature seen in the figure 4.16 in purple spheres.

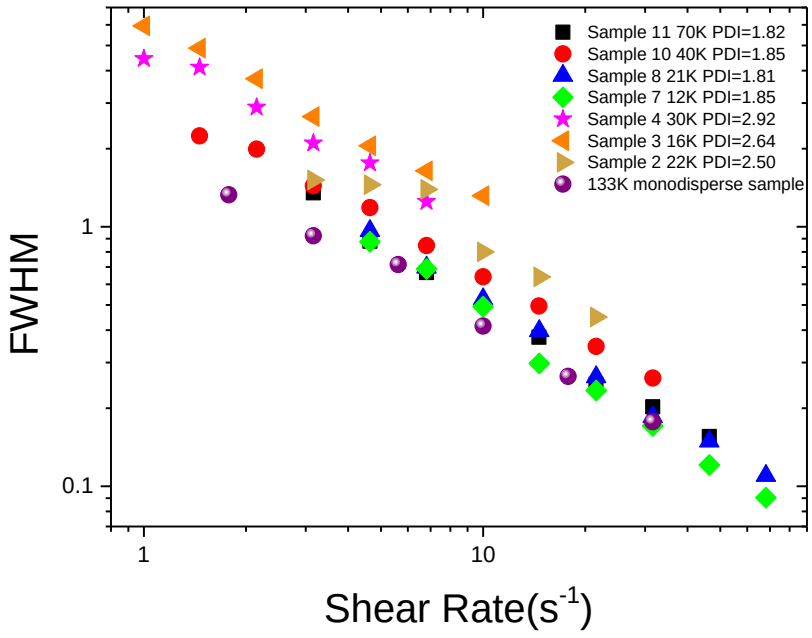

Figure 4.16. FWHM for all samples versus the shear rate, and a comparison with a monodisperse sample from literature(purple)

From the figure 4.16 above we can see that the data from the monodisperse sample in the literature collapse with those of our samples with the lowest polydispersity, but as the polydispersity of the sample increases, we observe an increase in the values of FWHM. For instance, SB3 and SB4 with polydispersity of 2.64 and 2.92, respectively, appears that have the highest values of FWHM. This is consequence of the fact that polydispersity affects the entanglements, and the effective flow-induced disentanglement process is weaker.

In continuation we plotted the FWM as a function of the Rouse Weissenberg number in figure 4.17. From the figure we can see that data follow the same trend as they did with the plot of FWHM as a function of the shear rate. Samples with the lowest polydispersity have low values of FWHM, whereas as the polydispersity of the samples increases the value of FWHM also increases.

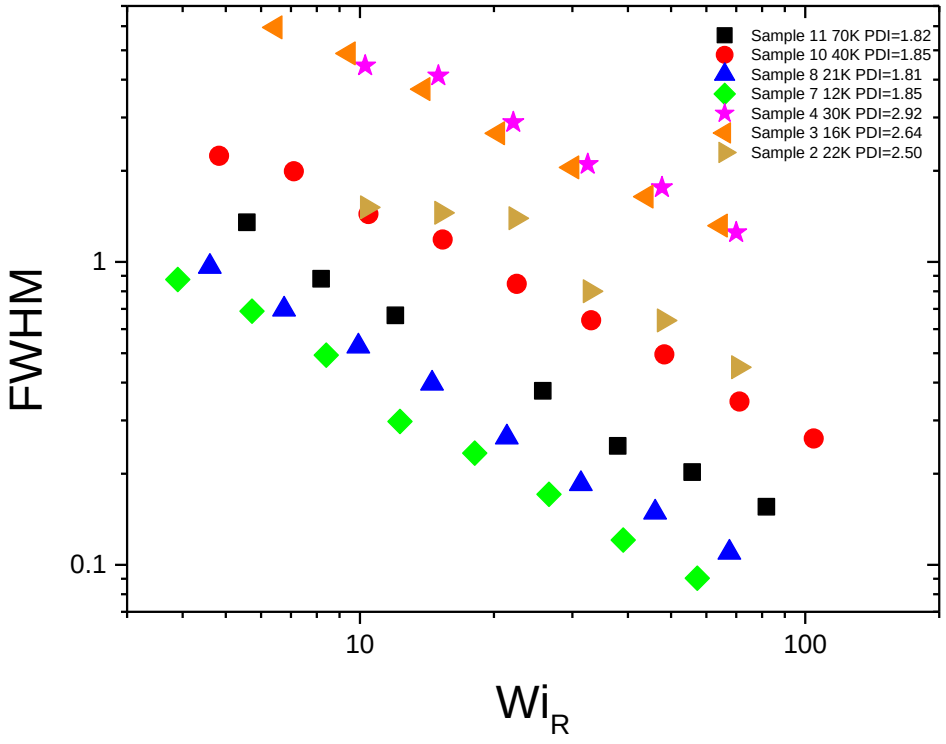

Figure 4.17. FWHM as a function of Rouse Weissenberg number.

The shear thinning behavior is clearly evidenced in the plot of the ratio of steady state viscosity by the zero-shear viscosity versus the Rouse Weissenberg number. Figure 4.18 shows that entangled and unentangled polymers represent two distinct groups. With the unentangled ones having a less sharp sheer thinning in comparison to the entangled ones. For the entangled systems, the slope of the high-shear-rate power law is -0.8[39]. For the unentangled polymers the slope is -0.5.

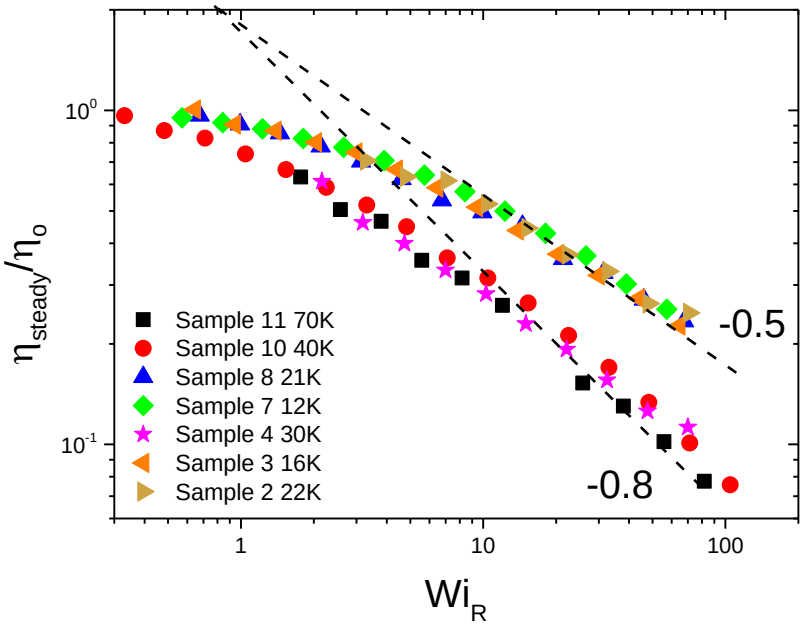

Figure 4.18. Ratio of Steady state viscosity and zero shear viscosity versus the Rouse Weissenberg number for all samples.

5. Conclusion

In this thesis we examined the linear and nonlinear rheological properties of linear polystyrene melts with varying molecular weight and molecular weight distribution (MWD). The molecular weight distribution was elegantly tailored by blending the pure components. The molar masses ranges from 3 to 70 kg/mol, and reasonably narrow molecular weight distribution (MWD), below 2. By mixing different polymers we obtain blends of different average MWD (up to 5.3). Samples ranged from unentangled, to barely entangled, and fully entangled regime. The absence of entangles, reflected into a significant brittleness of the material. This consideration, in addition to the high sensitivity of the rheological results to the presence of air in the specimens, called for a meticulous sample preparation and measuring protocol. We showed that the linear and nonlinear shear rheology significantly affected the MWD. For the linear rheological measurements, we presented sample master curves which are characterized by the absence of a plateau in the intermediate zone and of a rubbery plateau for the unentangled samples. In order to be sure that the time-temperature superposition (TTS) that was employed to build the master curves at a reference temperature holds, we built the Van Gurp-Palmen plots and we verified that TTS does hold for our samples. Additionally, the scaling behavior of the viscosity master curves revealed Zimm-like dynamics at early relaxation times that become Rouse-like at long relaxation times. We also calculated the zero-shear viscosity which is important for characterizing rheological response at low stress and for examining the influence of molecular architecture on resistance to flow. Our entangled samples do follow the scaling law predicted by the literature, whereas our unentangled blends with large polydispersity significantly deviate from the predicted slopes. This is not something that we didn't expect since as Graessley showed, the Doi Edwards tube model predicted a strong dependence of zero shear viscosity on MWD but for polydisperse systems it is essential to account for constraint release. Furthermore, we modelled our observed data with molecular models for both unentangled and entangled linear polymer chains. The experimental MWD of our samples was used as an input

parameter for the model. We found out that it is possible to describe the dynamics of entangled polymers with no fitting parameters, whereas for the unentangled MWD it followed that our samples represented good model system to test the molecular models with systems characterized by complex MWDs. Nonlinear step rate tests were also performed at different temperatures and shear rates and present scaling analysis for the nonlinear properties based on the characteristics of the transient signals as function of the Weissenberg number for the different samples. In the peak strain as a function of the Weissenberg number we observed that the entangled samples follow well-known Doi-Edwards's value of 2.3, whereas the unentangles polymers appears to have an increased slope. For the η_{max} over the η_{steady} versus the Rouse Weissenberg number we observed at low values of Weissenberg number that the data collapse at the value of 1. The entangled systems follow slope of 0.2, whereas for the unentangled systems they follow a slope of 0.1. For the FWHM as a function of the shear rate it was observed an overlap of our monodisperse samples with a monodisperse sample from the literature but as the polydispersity increased in the samples so did the value of the FWHM. Finally for the ratio of steady state viscosity by the zero-shear viscosity versus the Rouse Weissenberg number it was observed that the entangled systems follow a slope of -0.8 predicted by literature. To conclude we presented a detailed analysis of pure linear polystyrenes and their blends characterized by complex MWD combining linear and nonlinear shear rheology, differential scanning calorimetry and molecular modelling. We showed that blending linear polystyrenes to obtain complex MWD can significantly change the mechanical properties of melts.

References

(1) Barnes, H. A.; Hutton, J. F.; Walters, K. *An Introduction to Rheology*; Elsevier, 1989.
(2) Squeezing and Elongational Flow. *FOOD Eng.* 9.
(3) Malvern Instruments Limited. A Basic Introduction to Rheology. 2016.
(4) Thomas G. Mezger. *Applied Rheology*; 2015.
(5) Liu, Y.; Winter, H. H.; Perry, S. L. Linear Viscoelasticity of Complex Coacervates. *Adv. Colloid Interface Sci.* **2017**, *239*, 46–60. https://doi.org/10.1016/j.cis.2016.08.010.
(6) M. Rubinstein, Ralph H. Colby. *M. Rubinstein, Ralph H. Colby-Polymer Physics Chemistry-Oxford University Press, USA*; Oxford University Press, USA, 2003.
(7) The tube model https://cbp.tnw.utwente.nl/PolymeerDictaat/node62.html (accessed 2022 -02 -18).
(8) Chapter 7 Entanglements and Reptation https://www.eng.uc.edu/~beaucag/Classes/Physics/DynChapter7html/Chapter7.html (accessed 2022 -02 -18).
(9) Ruymbeke, E. V.; Liu, C.; Bailly, C. Quantitative Tube Model Predictions for the Linear Viscoelasticity of Linear Polymers.
(10) Dealy M, John , Ronald G. Larson. *Structure and Rheology of Molten Polymers*; 2006.
(11) Kissin, Y. V. Molecular Weight Distributions of Linear Polymers: Detailed Analysis from GPC Data. *J. Polym. Sci. Part Polym. Chem.* **1995**, *33* (2), 227–237. https://doi.org/10.1002/pola.1995.080330205.
(12) Nawab, Y.; Shahid, S.; Boyard, N.; Jacquemin, F. Chemical Shrinkage Characterization Techniques for Thermoset Resins and Associated Composites. *J. Mater. Sci.* **2013**, *48*, http://link.springer.com/article/10.1007%2Fs10853-013. https://doi.org/10.1007/s10853-013-7333-6.
(13) Snijkers, F.; Vlassopoulos, D. Cone-Partitioned-Plate Geometry for the ARES Rheometer with Temperature Control. *J. Rheol.* **2011**, *55* (6), 1167–1186. https://doi.org/10.1122/1.3625559.
(14) Costanzo, S.; Ianniruberto, G.; Marrucci, G.; Vlassopoulos, D. Measuring and Assessing First and Second Normal Stress Differences of Polymeric Fluids with a Modular Cone-Partitioned Plate Geometry. *Rheol. Acta* **2018**, *57* (5), 363–376. https://doi.org/10.1007/s00397-018-1080-1.
(15) Wang, S.-Q.; Ravindranath, S.; Boukany, P. E. Homogeneous Shear, Wall Slip, and Shear Banding of Entangled Polymeric Liquids in Simple-Shear Rheometry: A Roadmap of Nonlinear Rheology https://pubs.acs.org/doi/pdf/10.1021/ma101223q (accessed 2022 -02 -18). https://doi.org/10.1021/ma101223q.
(16) Tianhong, C. Preventing Wall Slip in Rheology Experiments. 2019.
(17) Tanner, R. I.; Keentok, M. Shear Fracture in Cone-Plate Rheometry. *J. Rheol.* **1983**, *27* (1), 47–57. https://doi.org/10.1122/1.549698.
(18) van Gurp, M.; Palmen, J. TIME-TEMPERATURE SUPERPOSITION FOR POLYMERIC BLENDS. 4.

(19) Williams, M. L.; Landel, R. F.; Ferry, J. D. The Temperature Dependence of Relaxation Mechanisms in Amorphous Polymers and Other Glass-Forming Liquids. *J. Am. Chem. Soc.* **1955**, *77* (14), 3701–3707. https://doi.org/10.1021/ja01619a008.
(20) Cho, K.-S. Geometric Interpretation of Time-Temperature Superposition. *Korea-Aust. Rheol. J.* **2009**, *21* (1), 13–16.
(21) Parisi, D.; Ahn, J.; Chang, T.; Vlassopoulos, D.; Rubinstein, M. Stress Relaxation in Symmetric Ring-Linear Polymer Blends at Low Ring Fractions. *Macromolecules* **2020**, *53* (5), 1685–1693. https://doi.org/10.1021/acs.macromol.9b02536.
(22) Gottlieb, M.; Macosko, C. W. The Effect of Instrument Compliance on Dynamic Rheological Measurements. *Rheol. Acta* **1982**, *21* (1), 90–94. https://doi.org/10.1007/BF01520709.
(23) Ferry, J. D. *Viscoelastic Properties of Polymers*; John Wiley & Sons, 1980.
(24) Rob Poole. The Deborah and Weissenberg Numbers. *Br. Soc. Rheol. Rheol. Bull.* **2012**.
(25) Mark, J. E.; Erman, B.; Roland, M. *The Science and Technology of Rubber*; Academic Press, 2013.
(26) An experimental appraisal of the Cox–Merz rule and Laun's rule based on bidisperse entangled polystyrene solutions - ScienceDirect https://www.sciencedirect.com/science/article/pii/S0032386104009814 (accessed 2022 -02 -15).
(27) van Ruymbeke, E.; Keunings, R.; Stéphenne, V.; Hagenaars, A.; Bailly, C. Evaluation of Reptation Models for Predicting the Linear Viscoelastic Properties of Entangled Linear Polymers. *Macromolecules* **2002**, *35* (7), 2689–2699. https://doi.org/10.1021/ma011271c.
(28) Parisi, D.; Costanzo, S.; Jeong, Y.; Ahn, J.; Chang, T.; Vlassopoulos, D.; Halverson, J. D.; Kremer, K.; Ge, T.; Rubinstein, M.; Grest, G. S.; Srinin, W.; Grosberg, A. Y. Nonlinear Shear Rheology of Entangled Polymer Rings. *Macromolecules* **2021**, *54* (6), 2811–2827. https://doi.org/10.1021/acs.macromol.0c02839.
(29) Milner, S. T.; McLeish, T. C. B. Reptation and Contour-Length Fluctuations in Melts of Linear Polymers. *Phys. Rev. Lett.* **1998**, *81* (3), 725–728. https://doi.org/10.1103/PhysRevLett.81.725.
(30) Likhtman, A. E.; McLeish, T. C. B. Quantitative Theory for Linear Dynamics of Linear Entangled Polymers. *Macromolecules* **2002**, *35* (16), 6332–6343. https://doi.org/10.1021/ma0200219.
(31) Des Cloizeaux, J. Relaxation and Viscosity Anomaly of Melts Made of Long Entangled Polymers: Time-Dependent Reptation. *Macromolecules* **1990**, *23* (21), 4678–4687. https://doi.org/10.1021/ma00223a028.
(32) Tsenoglou, C. Molecular Weight Polydispersity Effects on the Viscoelasticity of Entangled Linear Polymers. *Macromolecules* **1991**, *24* (8), 1762–1767. https://doi.org/10.1021/ma00008a012.
(33) Zimm, B. H. Dynamics of Polymer Molecules in Dilute Solution: Viscoelasticity, Flow Birefringence and Dielectric Loss. *J. Chem. Phys.* **1956**, *24* (2), 269–278. https://doi.org/10.1063/1.1742462.

(34) Shaw, M. T. On Estimating the Zero-Shear-Rate Viscosity: Tests with PIB and PDMS. *AIP Conf. Proc.* **2016**, *1779* (1), 070011. https://doi.org/10.1063/1.4965543.
(35) Graessley, W. W. Some Phenomenological Consequences of the Doi–Edwards Theory of Viscoelasticity. *J. Polym. Sci. Polym. Phys. Ed.* **1980**, *18* (1), 27–34. https://doi.org/10.1002/pol.1980.180180103.
(36) Polymer Molecular Weight - an overview | ScienceDirect Topics https://www.sciencedirect.com/topics/engineering/polymer-molecular-weight (accessed 2022 -02 -21).
(37) Santangelo, P. G.; Roland, C. M. Interrupted Shear Flow of Unentangled Polystyrene Melts. *J. Rheol.* **2001**, *45* (2), 583–594. https://doi.org/10.1122/1.1349711.
(38) Doi, M.; Edwards, S. F. Dynamics of Concentrated Polymer Systems. Part 4.—Rheological Properties. *J. Chem. Soc. Faraday Trans. 2 Mol. Chem. Phys.* **1979**, *75* (0), 38–54. https://doi.org/10.1039/F29797500038.
(39) Costanzo, S.; Huang, Q.; Ianniruberto, G.; Marrucci, G.; Hassager, O.; Vlassopoulos, D. Shear and Extensional Rheology of Polystyrene Melts and Solutions with the Same Number of Entanglements. *Macromolecules* **2016**, *49* (10), 3925–3935. https://doi.org/10.1021/acs.macromol.6b00409.